ERDC/CHL SR-20-3

US Army Corps
of Engineers®
Engineer Research and
Development Center

ERDC
ENGINEER RESEARCH & DEVELOPMENT CENTER

Dredging Operations and Environmental Research

Laboratory Evaluation of Aquablok™ Erosion Resistance: Implications for Geotechnical Applications

Anthony M. Priestas, John H. Hull, Reed Ellis, Charles F. McKenzie, and Joseph Z. Gailani

September 2020

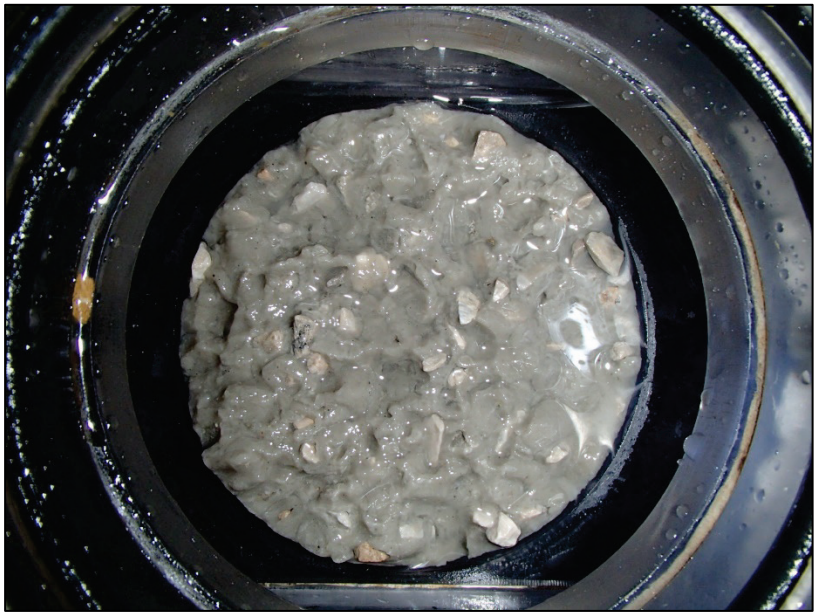

Coastal and Hydraulics Laboratory

The US Army Engineer Research and Development Center (ERDC) solves the nation's toughest engineering and environmental challenges. ERDC develops innovative solutions in civil and military engineering, geospatial sciences, water resources, and environmental sciences for the Army, the Department of Defense, civilian agencies, and our nation's public good. Find out more at www.erdc.usace.army.mil.

To search for other technical reports published by ERDC, visit the ERDC online library at https://erdclibrary.on.worldcat.org/discovery.

ERDC/CHL SR-20-3
September 2020

Laboratory Evaluation of Aquablok™ Erosion Resistance: Implications for Geotechnical Applications

Anthony M. Priestas, Charles F. McKenzie, and Joseph Z. Gailani
Coastal and Hydraulics Laboratory
US Army Engineer Research and Development Center
3909 Halls Ferry Road
Vicksburg, MS 39180-6199

John H. Hull and Reed Ellis
AquaBlok, Ltd.
175 Woodland Avenue
Swanton, OH 43558

Final report

Prepared for Dredging Operations and Environmental Research Program
Vicksburg, MS 39180

Under Project No. 485304, “Cost Effective Stabilization of Dredged Sediment for Capping and Nearshore Placement”

Abstract

AquaBlok™ (AB) is a commercial product traditionally used as an alternative material for contaminated sediment capping applications. Previous studies of AB capping performance have reported enhanced stabilization through increased erosion resistance. Subsequently, AB has been considered for use as an alternative levee repair material due to its cohesive properties. Through a series of laboratory experiments, this study investigated the erosion behavior of new AquaBlok formulations (10%, 20%, and 30% clay by weight) under increased shear stresses previously unachievable in the previous tests. The new AquaBlok formulations were tested in non-compacted and compacted states to simulate the physical properties in capping and levee repair applications.

In the non-compacted state, excess hydration of the clay matrix extended approximately 5 cm below the bed surface, which greatly reduced erosion resistance and was independent of clay percentage. Below this horizon, critical shear stress increased, and erosion rates decreased, with clay percentage, respectively. However, this does not consider a continuous change in hydration state when exposed to free water. In the compacted state, erosion rates were greatly arrested, with measureable erosion only possible under the maximum applied shear stress (24 Pa). The results are discussed in the context of capping and levee applications.

Contents

Figures and Tables

Figures

Tables

Preface

This study was conducted for the Dredging Operations and Environmental Research (DOER) Program under Project 485304, "Cost Effective Stabilization of Dredged Sediment for Capping and Nearshore Placement." The technical monitor was Dr. Joseph Z. Gailani.

The work was performed by the Field Data Collection and Analysis Branch of the Navigation Division, US Army Engineer Research and Development Center, Coastal and Hydraulics Laboratory (ERDC-CHL). At the time of publication of this report, Mr. William C. Butler was Chief of the Field Data Collection and Analysis Branch; Dr. Jacqueline S. Pettway was Chief of the Navigation Division; and Mr. Charles E. Wiggins was the Technical Director for Navigation. Dr. Todd S. Bridges was the Program Manager for DOER. The Deputy Director of ERDC-CHL was Mr. Jeffery R. Eckstein, and the Director was Dr. Ty V. Wamsley.

Additional funding for this study was supplied by AquaBlok, Ltd. under a Cooperative Research and Development Agreement.

The Commander of ERDC was COL Teresa A. Schlosser, and the Director was Dr. David W. Pittman.

1 Introduction

AquaBlok™, Ltd. manufactures a range of composite aggregate particle products used commercially in geotechnical and subaqueous applications. Geotechnical applications include the creation of anti-seep collars, cores for levees and dikes, and trench/breaker dams for pipeline installations, among other uses. In subaqueous applications, these products are commonly used to provide in situ sequestration and stabilization of contaminated sediments.

Subaqueous capping is a long-standing practice used to immobilize contaminated sediments and prevent contaminants from seeping into the overlying water column. As described by Palermo (1998), the capping materials vary from sand to gravel and may include the use of liners and geotextiles. The choice of material depends on cost, contaminant type, and site considerations—each choice offers certain advantages and disadvantages. For example, sands and gravels can be applied with minimal dispersion through the water column; they also deter bioturbation of the upper sediment layers and are physically more stable. However, these sediments are highly permeable, which can allow contaminants to migrate into the overlying water through consolidation and diffusion processes. Conversely, while fine-grained sediments are better chemical barriers (particularly clay-rich sediments), they are more easily bioturbated, have larger footprints due to dispersion, have reduced slope stability, and are prone to self-weight consolidation. Consequently, the sediment cap design would benefit from the dual function as an armoring agent (to resist wave-current erosion) and an isolating agent (to prevent contaminant migration). Engineered materials such as AquaBlok (AB) were designed to meet the dual function of armoring and isolation in capping applications.

1.1 Background

The AB composite was previously evaluated by multiple lab and field trials, including a detailed, 3-year lab and field demonstration conducted by researchers directed by the US Environmental Protection Agency (US EPA), as documented in a final report on Innovative Capping Technologies (US EPA 2007).

As part of that investigation, the US EPA contracted with the US Army Engineer Research and Development Center (ERDC), Coastal and Hydraulics Laboratory, to perform erosional shear stress studies using the ERDC, then newly developed, Sedflume device to evaluate erosion resistance of a particular AquaBlok product. For that study, cores collected from field-scale applications were tested in the Sedflume, having been collected at 6-months post-application and 30-months post-application. The testing results indicated that both performed similarly and that reported critical shear stresses ranged from 3 to 10 N/m^2* (Pascals/Pa), essentially maxing out the erosional limit effects of the Sedflume, at that time.

Subsequent to that testing, the ERDC laboratory upgraded its capabilities to erode cores at higher shear stresses (maximum of 24 Pa), and AquaBlok, Ltd. entered into a Cooperative Research and Development Agreement with ERDC to conduct additional erosion tests on new composite formulations using the upgraded device.

This report summarizes the laboratory work to determine the rates and thresholds of erosion for various AB formulations and that of a natural soil used for levee construction as a comparison. Based on the results, inferences are made to the performance of these materials in subaqueous capping and levee construction applications, and recommendations are made for future applications and further testing.

1.2 Objectives

The objectives of the research were two-fold. First, new formulations of AB were evaluated using the ERDC Sedflume to determine the relative erosion resistance for sediment capping applications in a non-compacted state; these results were compared to prior testing performed by the ERDC for the US EPA Superfund Innovative Technology Evaluation (SITE) project that studied an early formulation of AB. Second, a specific formulation of AB (AB-1585) was tested in a compacted state for direct comparison against a natural soil from an approved borrow source for levee repair and

* For a full list of the spelled-out forms of the units of measure used in this document, please refer to *US Government Publishing Office Style Manual*, 31st ed. (Washington, DC: US Government Publishing Office 2016), 248-52, https://www.govinfo.gov/content/pkg/GPO-STYLEMANUAL-2016/pdf/GPO-STYLEMANUAL-2016.pdf.

construction. The goal of this second test was to compare the erosion resistance of AB-1585 using simulated levee construction approaches against a conventional soil used in levee repair and potentially subjected to scouring forces from overtopping during flood events, etc.

1.3 Approach

A series of experiments using the Sedflume erosion device were conducted on laboratory-generated cores of AB and a natural soil to evaluate their erosion characteristics. The erosion rate data were modeled using a power-law relationship to estimate the critical shear stress and provide erosion parameters. The results are first discussed in terms of factors that contribute to or inhibit erodibility, then interpreted in the context of aforementioned engineering applications.

2 Materials and Methods

2.1 AquaBlok (AB) description

In its basic form, AB consists of a stone core encapsulated by swelling clays and polymers. In sediment capping applications, the product is applied through the water column and allowed to self-compact as the clay mineral components hydrate and swell, forming a cohesive layer over sediment surfaces (Figure 1).

Figure 1. Graphic representation of AB applied as a capping material. Modified from Hull et al. (1999).

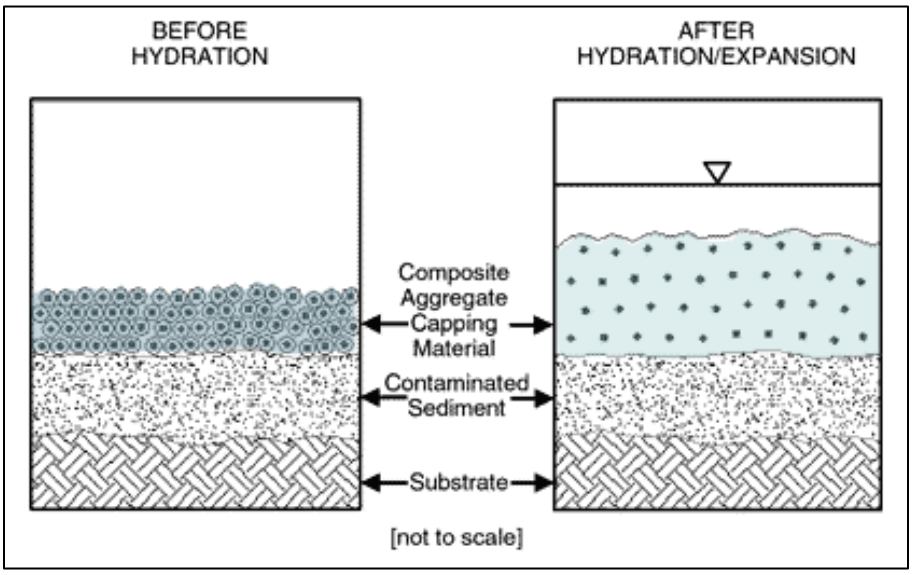

AB formulations are labeled according to the weight percent of clay relative to the aggregate particles. Thus, the formulations labeled as AB-1585, AB-2080, and AB-3070 correspond to 15%, 20%, and 30% clay, respectively. The particle sizes of all aggregate formulations tested were generally graded as #8 gravel (sizes 3/8 in. to 1/2 in.). Proprietary formulations (mixtures of aggregate, clay type, and polymer) are designed by the manufacturer for both fresh and saltwater applications; freshwater versions were used for all testing reported herein. Examples of AquaBlok products are shown in Figure 2.

Figure 2. Overview of the AquaBlok products AB-1585 (left) and AB-2080 (right).

2.2 Erosion testing

2.2.1 Sedflume apparatus and test procedure

Sedflume, originally developed by researchers at the University of California at Santa Barbara (McNeil et al. 1996), is an experiment apparatus designed to quantify cohesive sediment erosion (Figure 3). Using this apparatus, the erodibility of a sediment is quantified as the change in bed surface elevation over time, or erosion rate due to an applied bed shear stress. Other researchers (e.g., Akahori et al. 2008) have used the term erosion velocity to distinguish it from mass erosion rate. The flume channel is 80 cm long with a cross section of 2 × 10 cm and is constructed of clear polycarbonate so erosion can be observed by the operator. The test section of the flume accepts 10 cm diameter cores up to 80 cm in length. Sediment cores can be extracted from natural settings (direct push cores) or created in the laboratory (remolded cores). Fully developed, smooth-turbulent flow is generated using a gas-powered centrifugal pump and is introduced to the core within the test section. The flow rate is monitored using a magnetic flow meter and is related to bed shear stress with empirical relationships previously calibrated using particle imaging velocimetry (Figure 3, inset). The bed shear stress (τ_b) is

the fluid force per unit area, measured in units of Pascal (Pa), exerted on the surface in the direction of flow.

Figure 3. Diagram of a Sedflume erosion testing device and example of recorded erosion data.

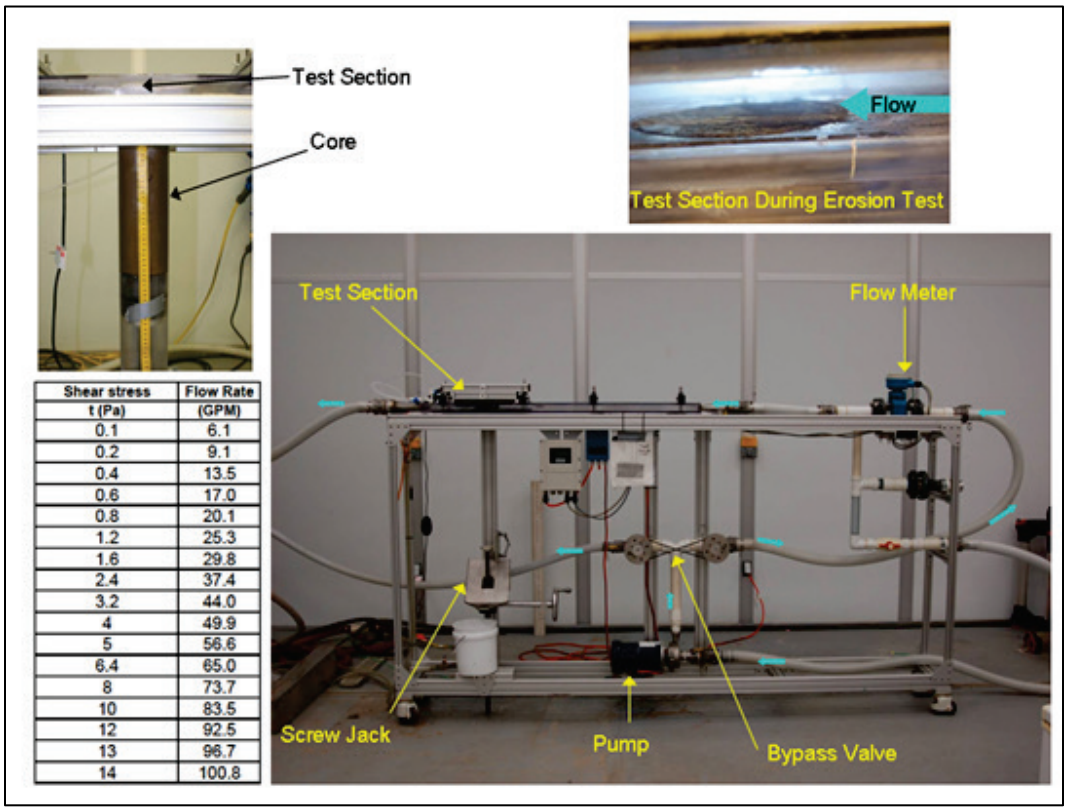

Shear stress t (Pa)	Flow Rate (GPM)
0.1	6.1
0.2	9.1
0.4	13.5
0.6	17.0
0.8	20.1
1.2	25.3
1.6	29.8
2.4	37.4
3.2	44.0
4	49.9
5	56.6
6.4	65.0
8	73.7
10	83.5
12	92.5
13	96.7
14	100.8

To perform erosion tests, cores are introduced to the test section (Figure 3). The surface of the core is made flush with the bed of the channel, and flow is gradually increased using a bypass valve. Erosion is initiated once the flow rate exceeds the critical stress for erosion. As erosion continues, cores are advanced manually using a screw jack to maintain the position of the core surface with the flume bed. Erosion rates are quantified using a graduated tape (read to the nearest 0.5 mm) and stopwatch. The erosion rate is calculated as the length of core eroded over an interval of time. Shear stress values were selected by trial and adjusted according to the observed erosion behavior. The intent of this procedure is to capture relative low, mid, and high erosion rates for the calculation of the critical stress and erosion parameters with error estimates.

Erosion tests were conducted for two material states: non-compacted and compacted. The non-compacted erosion tests were designed to evaluate erosion resistance when used as submerged, engineered fill (e.g.,

subaqueous cap). Conversely, the compacted erosion tests was designed to evaluate erosion resistance while in a highly compacted state (such as used in levee and dike construction). Compacted erosion was performed on both AB and a natural, clay-rich soil for comparison of the two materials. Table 1 lists the schedule of core preparation and test activities.

Table 1. Timeline of test procedure activities to include sample preparation for remolded cores, density scans to determine relative core competency, and Sedflume erosion testing.

Activity	Date (2017)
Non-Compacted Erosion Tests	
AB-1585 & AB-2080 core creation	10/13
AB-3070 core creation	10/16
AB-1585 density scan	10/16
AB-2080 & AB-3070 erosion tests	10/17 – 10/19
AB-1585 erosion tests	10/17 – 10/20
AB-3070 erosion tests	10/18 – 10/23
Compacted Erosion Tests	
Moisture adjustments	12/11
AB-1585 & WB Core creation	12/12
WB density scan	12/13
WB erosion tests	12/14 – 12/15
AB-1585 density scan	12/14
AB-1585 erosion tests	12/15

2.2.2 Non-compacted core preparation and erosion test procedure

Six remolded cores were created in the laboratory for testing, one for each AB formulation plus one replicate to be used if needed. To prevent size separation and gradation, the product was introduced to the core tube as quickly as possible using a wide-mouth funnel and a series of 8 cm lifts (Figure 4). While this method of core construction was intended to approximate a field application of AB, a true field application would involve the size separation of particles caused by differential settling. However, this was intentionally avoided in the laboratory to maintain an approximately constant bulk density with depth.

The AB was allowed to hydrate for 15 min before introducing the next lift. Six lifts created core lengths of approximately 45 cm. After completion, approximately 8 cm of standing water remained above the core surface. The cores were stored upright at room temperature until erosion began, approximately 1–3 days later (Table 1).

Figure 4. (A) Overview of the AB-2080 formulation, (B) polyvinyl chloride cup used to obtain an 8 cm lift, and (C) in-progress core preparation of AB-1585 and AB-2080 formulations.

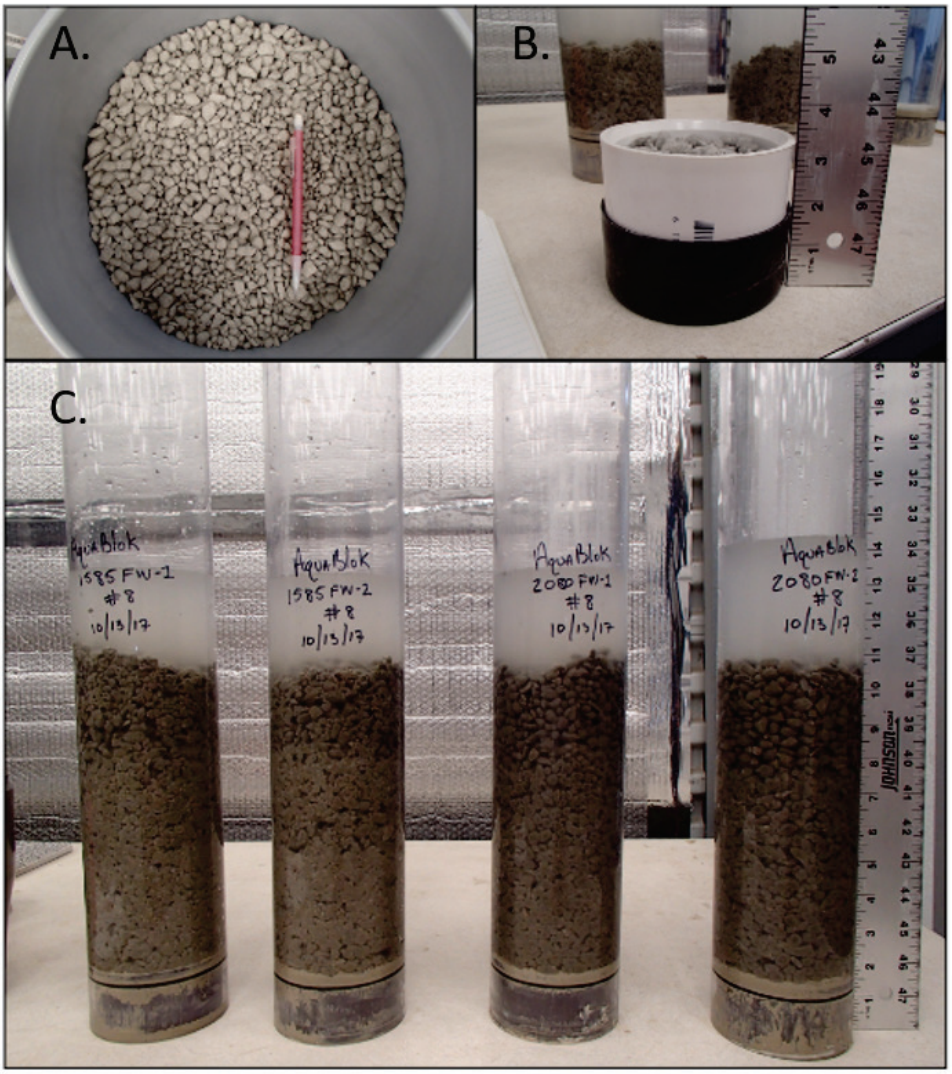

In some instances, there was not sufficient time to complete the erosion testing in single day. In that case, the core was removed from the flume, and the upper 2 cm of material that normally protrudes above the core barrel (the distance between top of the core barrel and the bottom of the flume test section) was removed, and the core barrel was capped. This was

done to minimize changes in the material properties due to prolonged exposure to air or water, which would alter the erosion behavior.

2.2.3 Compacted core preparation and erosion test procedure

Materials for the compacted erosion tests consisted of AB-1585 and a natural soil derived from pit 5 of the Willow Bend (WB) mine, a borrow area located in Edgard, Louisiana.

The WB soil was classified as a fine-grained, fat clay (CH, Unified Soil Classification System) with high plasticity (49%–79%) and low (< 3%) organic content*. The percent mass passing the No. 200 sieve was generally 94%–98%.

The optimum moisture content for each material was determined using the standard Proctor test (Method A) conducted by the ERDC Coastal and Hydraulics Laboratory Sediment Laboratory prior to core preparation. The optimum moisture content is the percent mass of water such that a soil's bulk density is maximized under compaction. Results gave optimum moisture contents of 15% and 23% for AB-1585 and the WB soil, respectively.

To prepare the compacted cores, the moisture contents of the AB and WB materials were adjusted to their optimum moisture contents. First, the materials were placed in tared aluminum trays, and a spray bottle was used to apply water gradually while mixing until a target soil weight (and therefore moisture content) was achieved (Figure 5). The materials were then sealed in plastic bags and left to stand for 24 hr to absorb the added water.

*Burns Cooley Dennis, Inc. Unpublished data. Geotechnical and Materials Engineering Consultants, Jackson, MS. 2008.

Figure 5. Material state of AB-1585 (top) and WB soil (bottom) prior to creating the compacted cores.

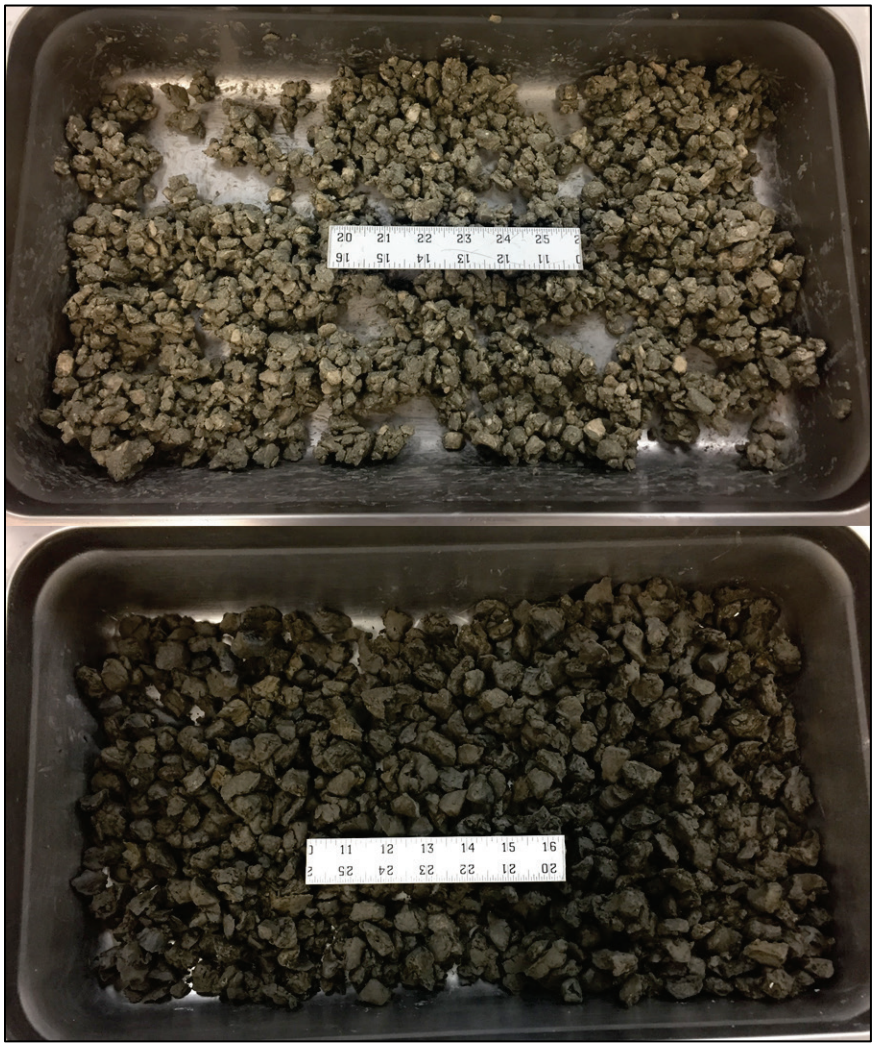

The cores were created directly within 4 in. polycarbonate tubes using 10 cm lifts and then compacted with the same mechanical effort. Each lift was compacted using 25 blows from a 2.5 kg (5.5 lb) hammer dropped from a height of 12 in., analogous to the standard Proctor procedure highlighted in ASTM D698 (ASTM 2012) (Figure 6). The total core lengths created were 18 cm for AB-1585 and 24 cm for the WB soil.

Figure 6. Example of the compaction process used in creating the compacted cores for AB-1585 (A and B) and WB soil (C and D).

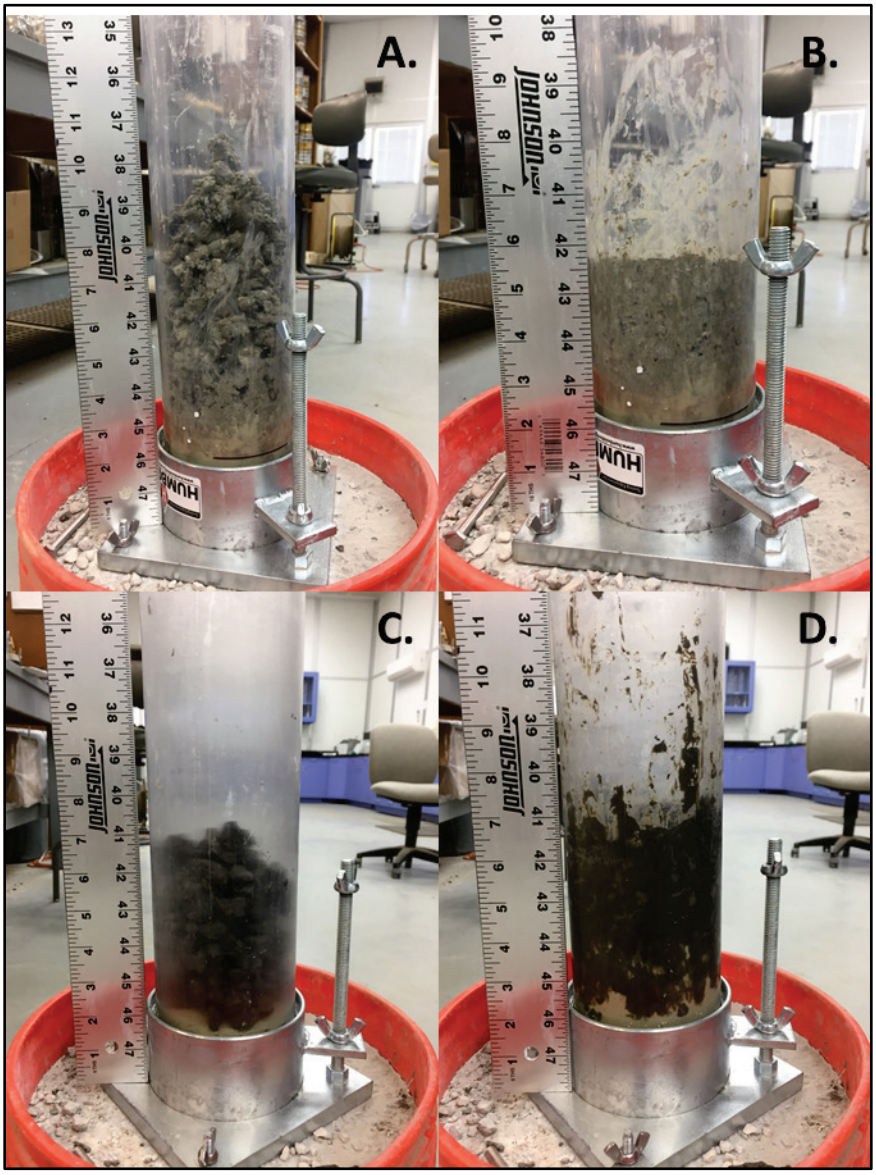

After compaction, the surface of the AB core was planar but had some roughness caused by small, pulverized rock fragments. However, the surface of the compacted WB soil was jagged and highly irregular (Figure 7A). During erosion testing within Sedflume, increases in surface roughness will increase apparent erosion rates caused by flow disturbance and erosion due to form drag. Therefore, the upper 4 cm was extruded and cut with a wire so that the upper surfaces of the AB and WB cores were relatively planar and initial conditions were as comparable as possible (Figure 7B).

A total of four compacted cores were created for testing—one for each material type (AB-1585 & WB) and respective replicates to be used if needed.

Figure 7. Compacted core surface of the WB soil (A) and after removal of the upper 4 cm (B).

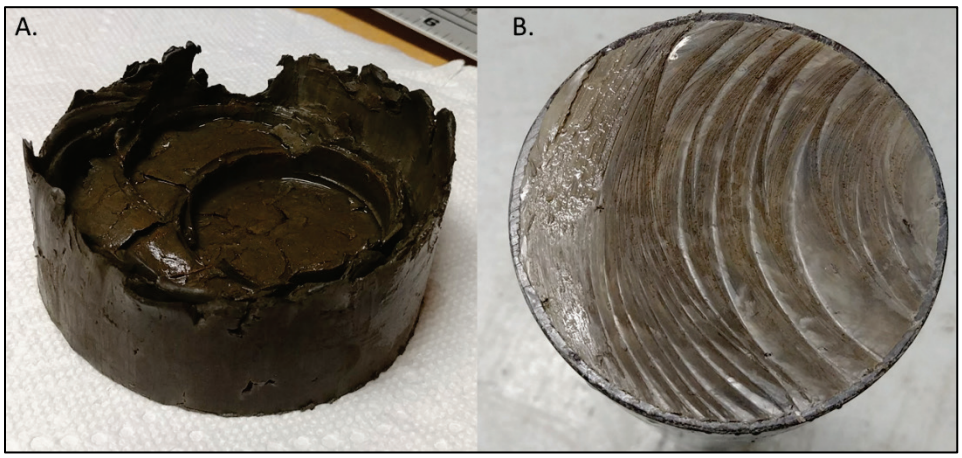

2.3 Density scans

Prior to erosion testing, bulk density profiles were generated for all cores using the ERDC X-Ray Attenuation (XRA) device. The density scans were used to evaluate the relative competency of prepared cores and note any discontinuities that might affect the erosion data. Details on the XRA and its operating principle can be found in Appendix A.

Cores were scanned at three intervals: an upper, middle, and lower section. Scan resolutions were programmed to be finer near the surface then coarsen with depth (Table 2). This is because the greatest density changes typically occur near the surface. Since significant density changes were not expected at depth, coarser scan resolutions were sufficient to capture density trends while saving time. Density profiles are provided in the results section.

Table 2. Scanning intervals for XRA density profiles. Core IDs appended with "C" correspond to compacted cores.

Core ID	AB-1585	AB-2080	AB-3070	AB-1585-C	WB-C
Depth interval @ scan resolution	0-5 cm @ 1 mm	0-5 cm @ 1 mm	0-5 cm @ 1 mm	0-6 cm @ 1 mm	0-5 cm @ 1 mm
	5-15 cm @ 2 mm	5-15 cm @ 2 mm	5-15 cm @ 2 mm	6-8 cm @ 2 mm	5-15 cm @ 2 mm
	15-25 cm @ 5 mm	15-25 cm @ 5 mm	15-25 cm @ 5 mm	—	15-25 cm @ 5 mm

2.4 Data analysis

Erosion rates are calculated directly from the raw data. Erosion rates of zero (no measureable erosion) are filtered out before data analysis. Here, the critical stress is defined as the shear stress that causes an erosion rate (E) of 10^{-4} cm/s (Roberts et al. 1998). This value represents a small but measureable erosion rate that reduces ambiguity about the threshold obtained from visual observations alone. Previous work (Lick et al. 2007) has shown that erosion rate as a function of bed shear stress can be modeled using the power law relation:

$$E = A\tau^n \tag{1}$$

where

E = erosion rate (cm/s)
τ = bed shear stress (Pa)
A = empirical constant
n = empirical exponent.

The parameters A and n are found by linearizing Equation 1 and fitting a robust linear regression model (i.e., not as affected by outliers) to the data. Critical stress, τ_{cr}, is then found by extrapolating the fitted linear regression model to $E = 10^{-4}$ cm/s.

3 Results

Erosion test results are presented separately for non-compacted and compacted cores.

3.1 Non-compacted cores

3.1.1 General observations

Figure 8 is a composite image of the three cores that shows their physical state just prior to erosion testing. All thee cores present abundant voids throughout except near the upper surfaces (Figure 9).

Figure 8. State of the non-compacted cores just prior to erosion testing for (A) AB-1585, (B) AB-2080, and (C) AB-3070.

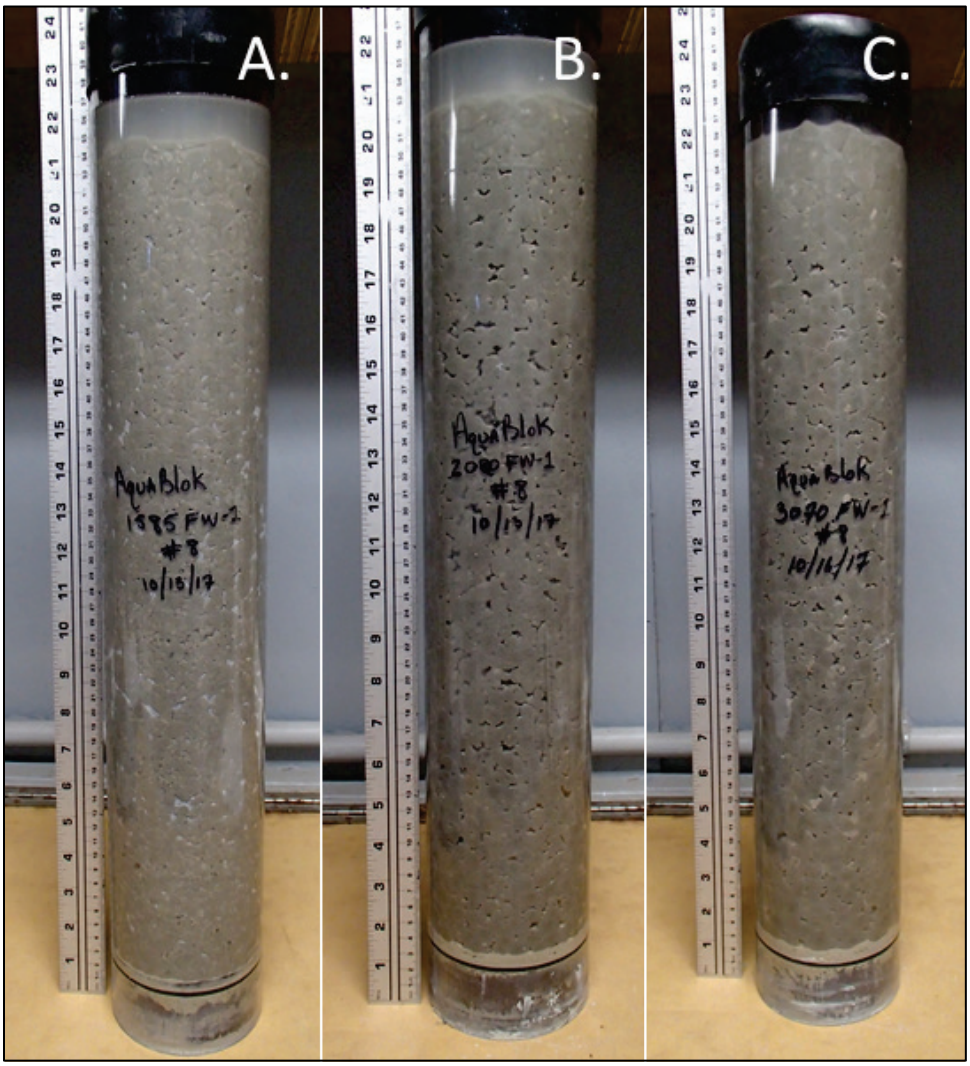

Here, the clay matrix in the upper 5–6 cm reached a change in material state related to the absorption of overlying water. The hydration and swelling of the clays caused a pore-filling behavior (Figure 9), which significantly decreased the bulk density as measured by XRA (Figure 10); the bulk density of the upper 5 cm gradually increases from a value of 1.0 g/cm^3 to approximately 1.4–1.5 g/cm^3. Below 5 cm, the bulk density increases slightly then stabilizes to a mean value of approximately 1.6–1.7 g/cm^3 for all formulations tested. The only significant difference between the density profiles is the larger apparent variability in the AB-3070 formulation, which is likely due to increased void space.

The significant change in material condition between the upper and lower sections of the cores drastically changed their erosion resistance. Since the erosion behavior of the upper layers is distinct from that of the lower layers, data from the upper 5 cm of each core were analyzed separately so as not to bias the derived erosion parameters of Equation 1, and the results of the two layers are herein presented separately.

Figure 9. Close up of the AB-1585 core upper-layer region (approximately 0–5 cm core depth) where the clays have absorbed significant water resulting in a lowered bulk density.

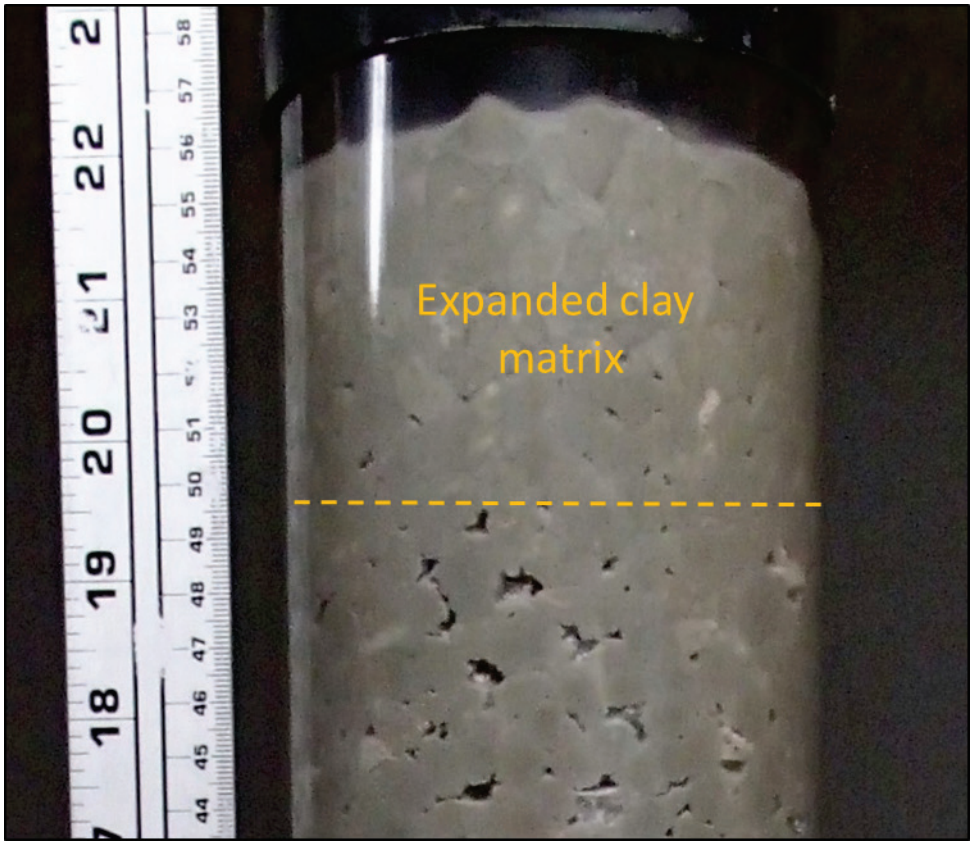

Figure 10. Density profiles with depth below core surface as measured by XRA. The highlighted areas show the pronounced decrease in density due to water absorption of the clay matrix.

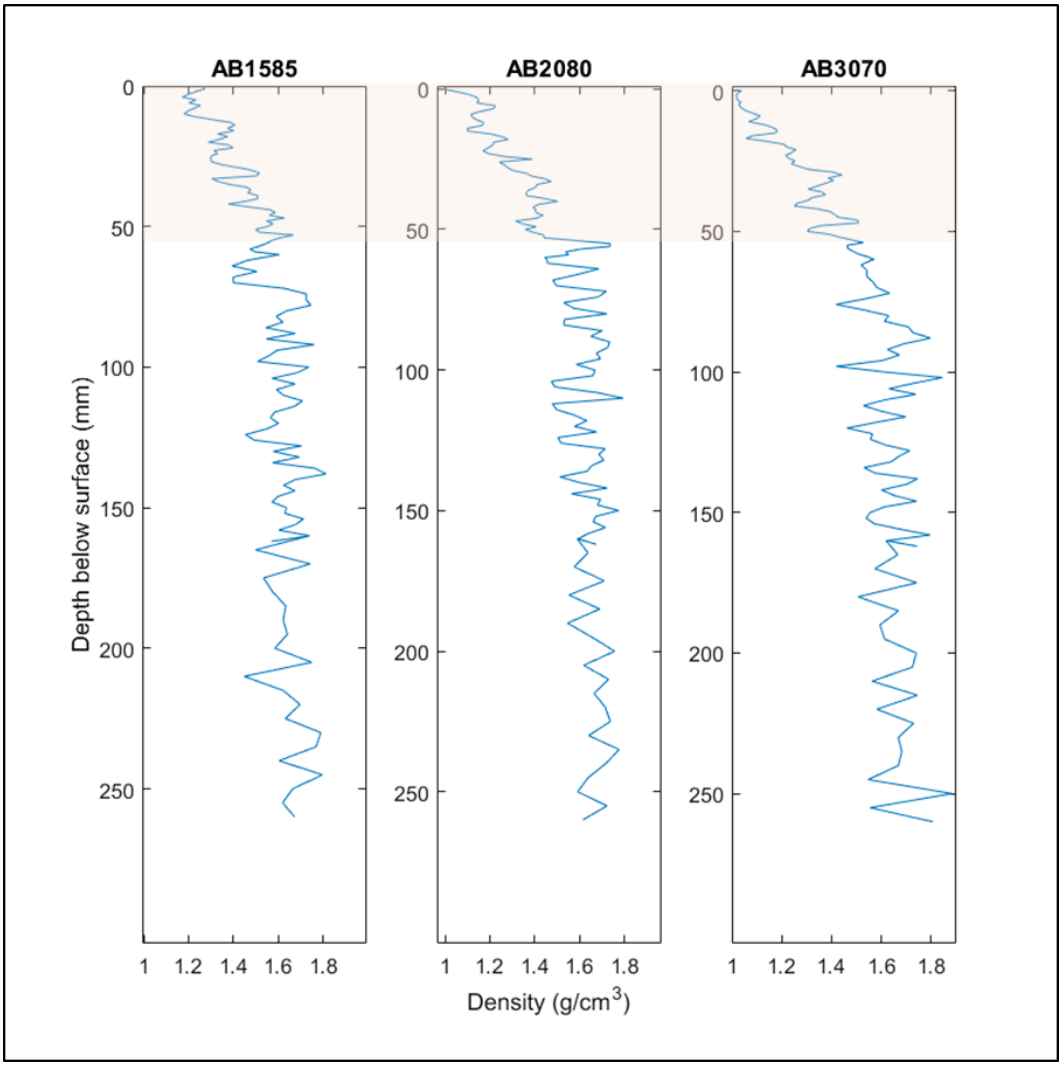

3.1.2 Erosion test results

3.1.2.1 Upper layer

A primary observation made during erosion testing pertains to the pronounced difference in erosion behavior between the hydrated upper region (approximately 0–5 cm) and the region below 5 cm. The exposure of swelling clays (in this case, sodium bentonite) to free water above the core surface resulted in significantly different erosion characteristics than the lower layers.

The erosion behavior of the hydrated upper region was similar for all three cores. In each case, the upper layer had absorbed enough water to reach a

visibly gelled state. In this state, granule-sized and larger stones could easily slide through the clay matrix, and mud aggregates eroded as viscous blebs at shear stress conditions ranging from 0.2 to 0.4 Pa. Notably, increasing the flow to 1.0 Pa typically resulted in a rapid erosion rate. The stark difference in erosion behavior between the upper and lower layers is demonstrated in Figures 11-13.

Figure 11. Core AB-1585 erosion rate versus shear stress. Symbol color indicates depth of measurement below the core surface. Upper layer fit is in blue, and lower layer fit is in orange, each with 95% confidence intervals.

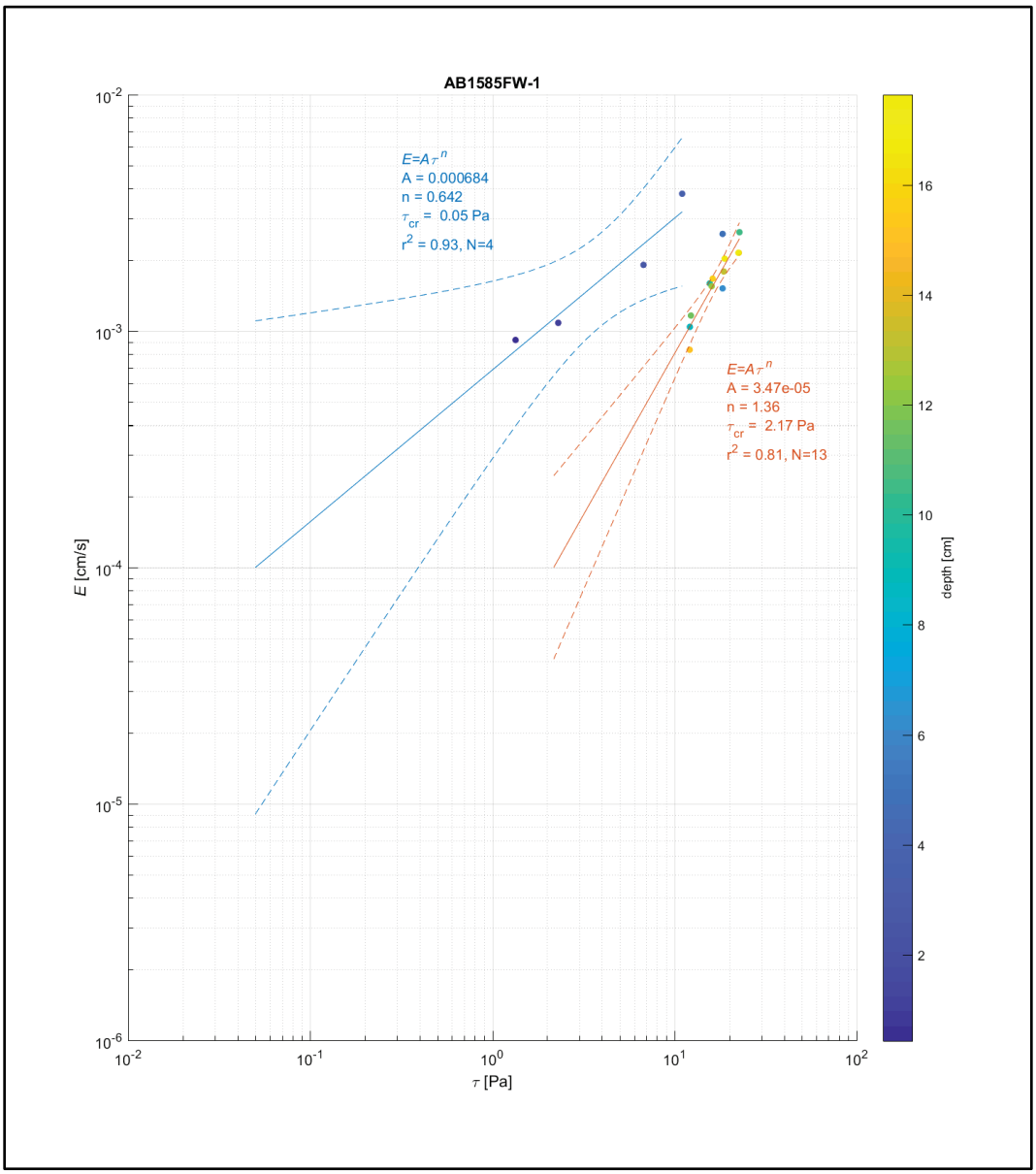

Figure 12. Core AB-2080 erosion rate versus shear stress. Symbol color indicates depth of measurement below the core surface. Upper layer fit is in blue, and lower layer fit is in orange, each with 95% confidence intervals.

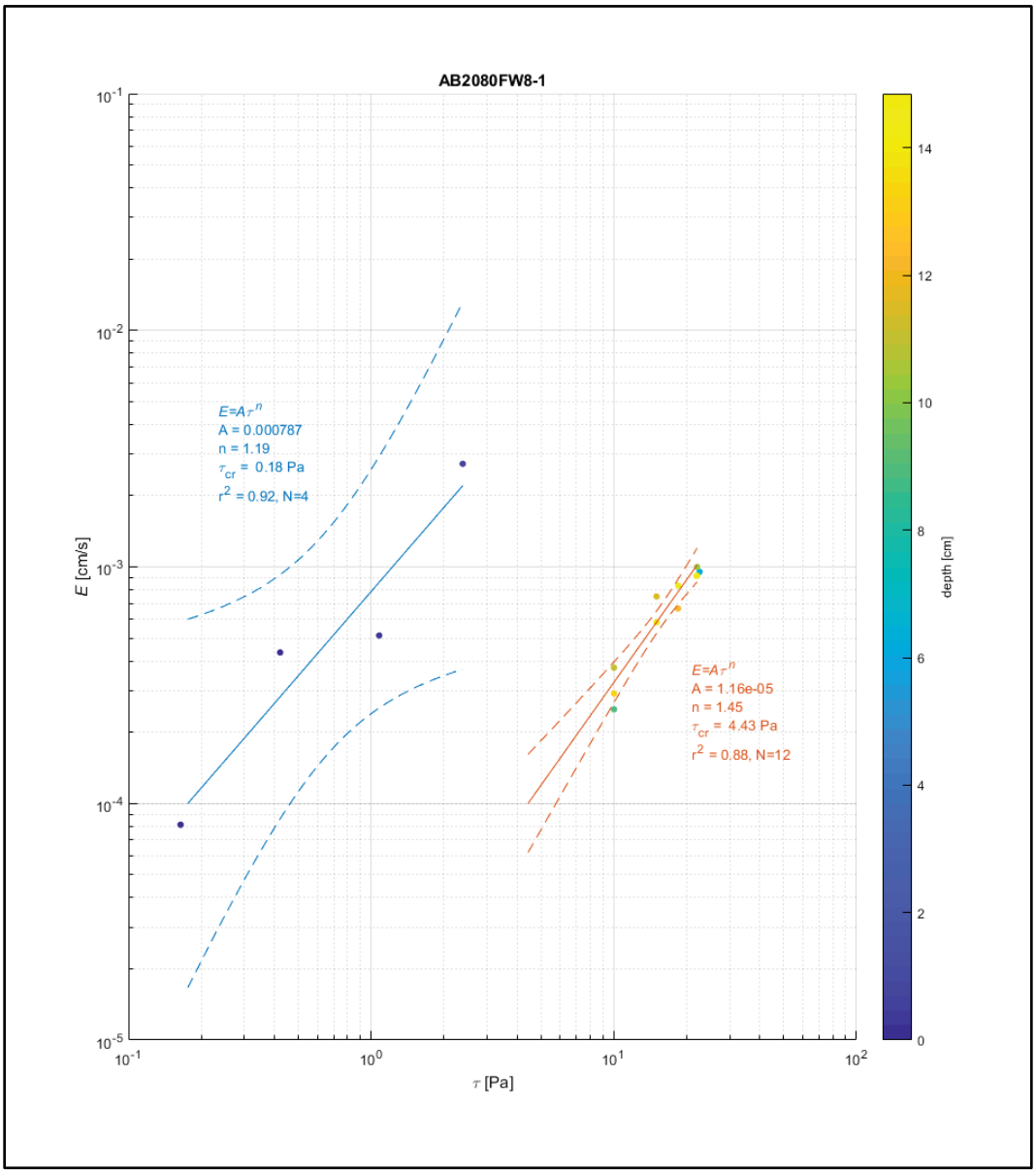

Figure 13. Core AB-3070 erosion rate versus shear stress. Symbol color indicates depth of measurement below the core surface. Upper layer fit is in blue, and lower layer fit is in orange, each with 95% confidence intervals.

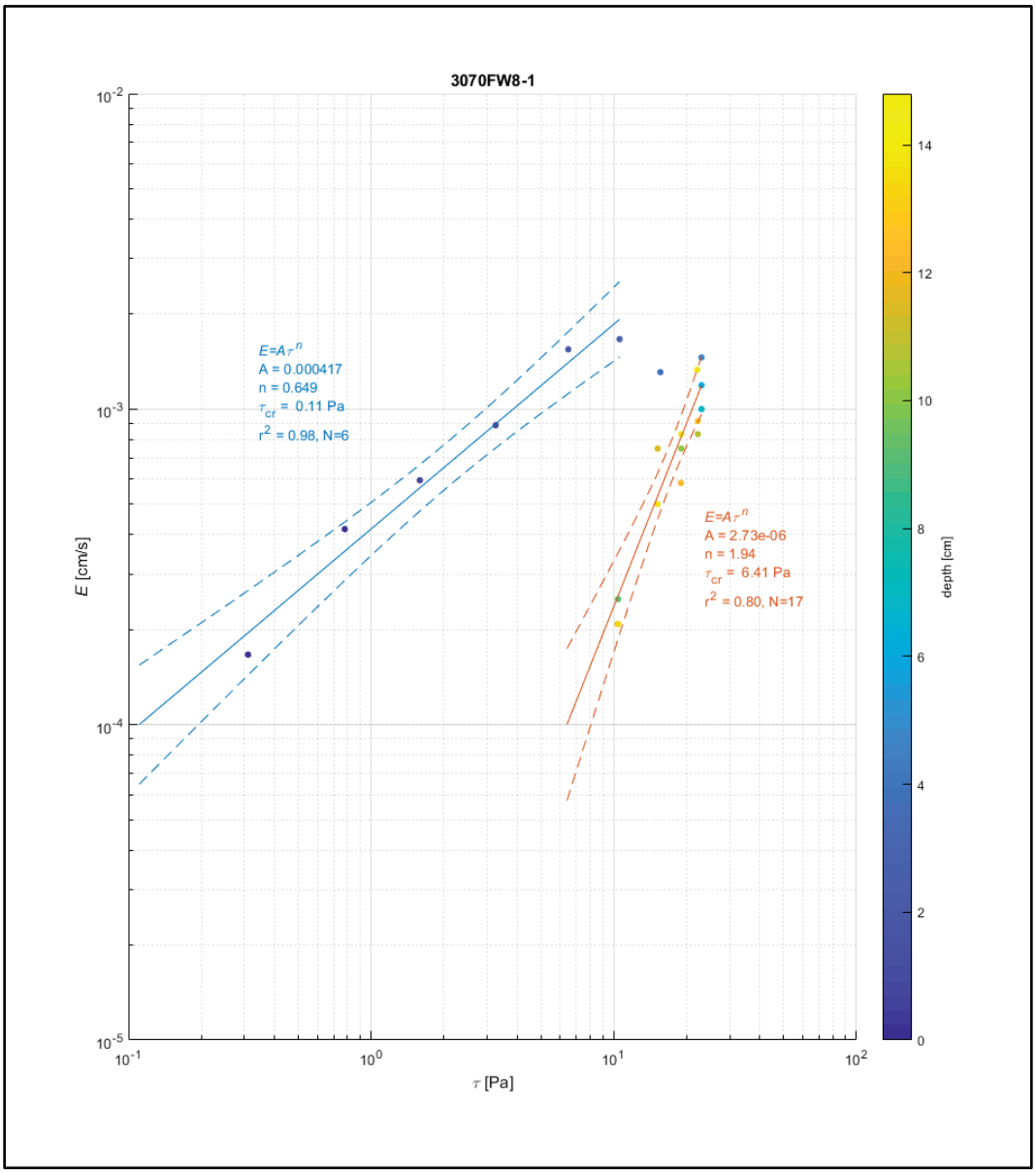

Since the erosion behavior of the upper layers was similar for each AB formulation, data from the upper layer were merged to represent average erosion characteristics (Figure 14). From this, the average critical shear stress of the upper layer was determined to be 0.11 Pa with a range of 0.08–0.16 Pa (Table 3). Consequently, erosion rates of the upper layer are predicted to be approximately 4×10^{-4} cm/s (or nearly 2 cm/hr) at a constant shear stress of 1.0 Pa. However, more data would be needed to fully understand the erosion behavior of this layer and better constrain the variability between the different AB formulations.

Figure 14. Average erosion characteristics of AB. Erosion versus shear stress for all data in the upper layer region of cores AB-1585, AB-2080, and AB-3070. Symbol color indicates depth of measurement below the core surface.

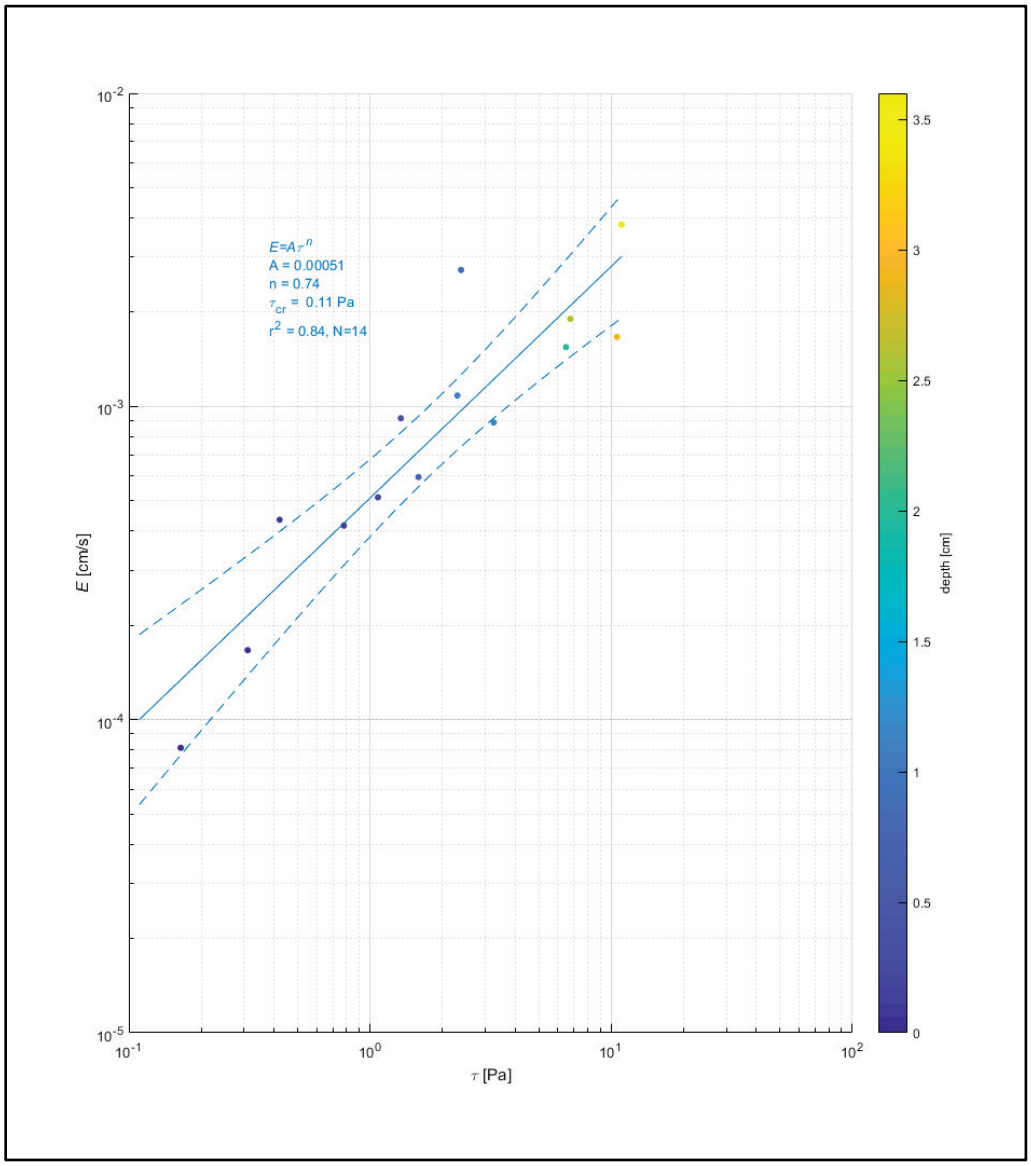

3.1.2.2 Lower layer

The erosion behavior of the lower layers was quite different from the upper layers. Due to the increased clay stiffness, surface erosion occurred as winnowing of the clay matrix that would expose the gravel in time. Eventually, enough of the surface area of the gravel would be exposed to flow for drag forces to overcome the cohesive strength of the buried portion of the gravel. More aggressive erosion occurred in situations where escaping gas was observed to be prevalent (due to voids; see Figures 8 and 9), causing larger aggregates of gravel and clay matrix to be dislodged together. Qualitatively, erosion rates appeared to decrease as the run progressed under a given shear stress. In other words, it was noted that in many instances, much of the measured erosion was induced at the beginning of a run. This appeared to be associated with the transition between the upper and lower layers beyond which the erosion behavior consisted of a slow winnowing of the matrix followed by occasional to intermittent gravel erosion.

Erosion rates of the lower layers were significantly less than that of the upper layers. The erosion behavior below 5 cm depth showed high erosion resistance for each AB formulation—the lowest critical shear stress from any formulation in this layer was 2.17 Pa. Likewise, the critical shear stress generally increased with increased clay proportions: 2.17 Pa for AB-1585, 4.34 Pa for AB-2080, and 6.84 Pa for AB-3070. From Figure 15, the erosion behaviors between AB-2080 and AB-3070 were very similar and more erosion resistant while the AB-1585 formulation was less erosion resistant.

Figure 15. Erosion rate versus shear stress for the lower layers (> 5 cm below surface) of AB-1585, AB-2080, and AB-3070. Symbol color indicates depth of measurement.

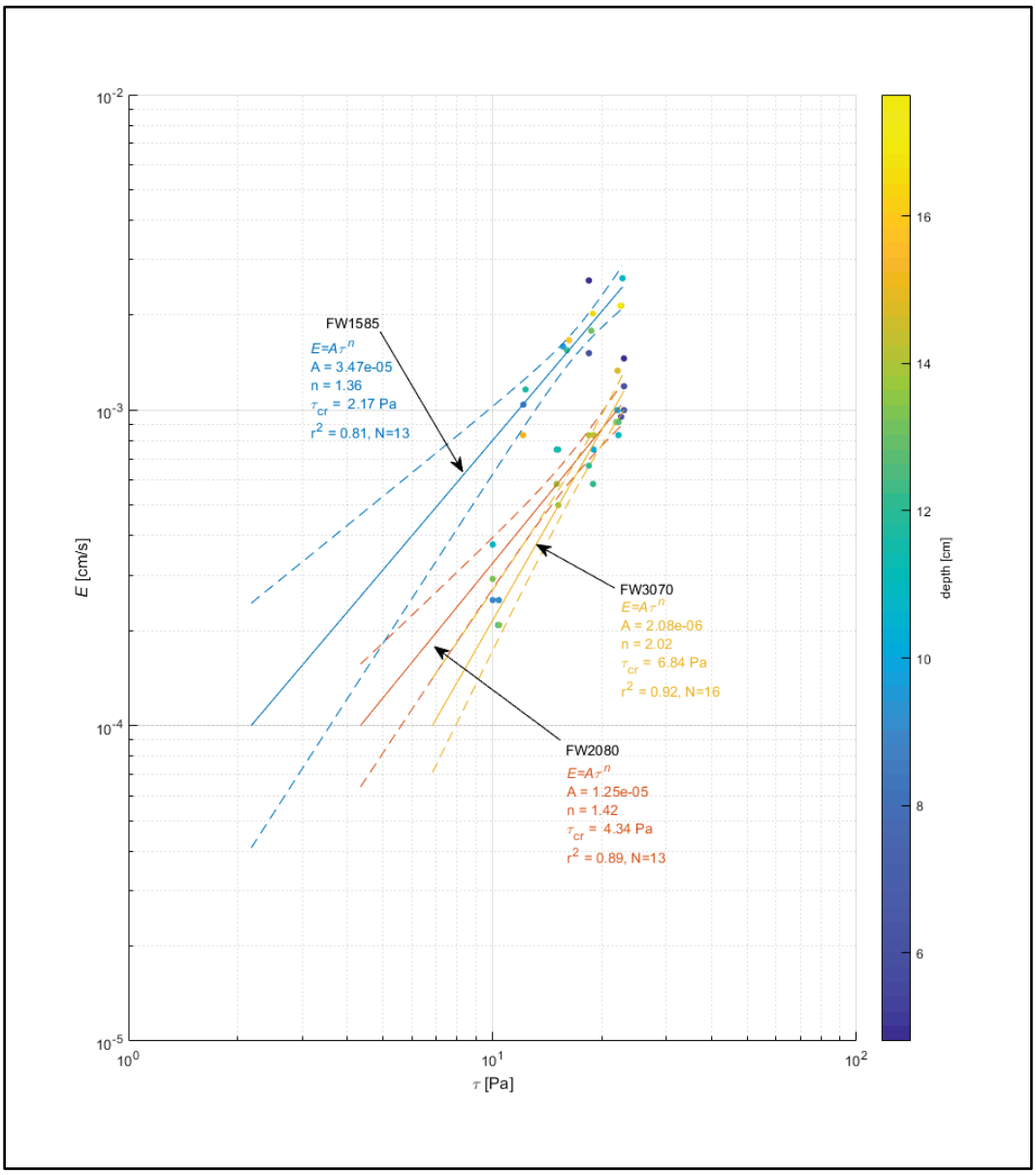

The slopes of the model fits (controlled by the parameter n in Equation 1) are indicators of the erosion rate magnitude predicted under a given shear stress. Figure 16 compares model fits of the upper layers (dashed lines) to those of the lower layers (solid lines) and illustrates the marked differences in their erosion behaviors. In the lower layer, higher values of n are associated with increased clay content (15, 20, 30). For example, a shear stress of 1.0 Pa is predicted to induce erosion rates of 1.3 and 0.5 mm/hr for AB-1585 and AB-2080 formulations, respectively, while the erosion rate for AB-3070 reduces to 0.07 mm/hr under the same shear

stress. However, confidence intervals are large in this region due to the uncertainty of the fit at shear stresses less than 10 Pa caused by lack of data control (Figure 15). Nonetheless, the data suggest that AB-3070 is approximately 18 times more erosion resistant than AB-1585.

Figure 16. Comparison of model fits for the upper layers (dashed lines) and lower layers (solid lines) for all three AB formulations. Model fit parameters are provided.

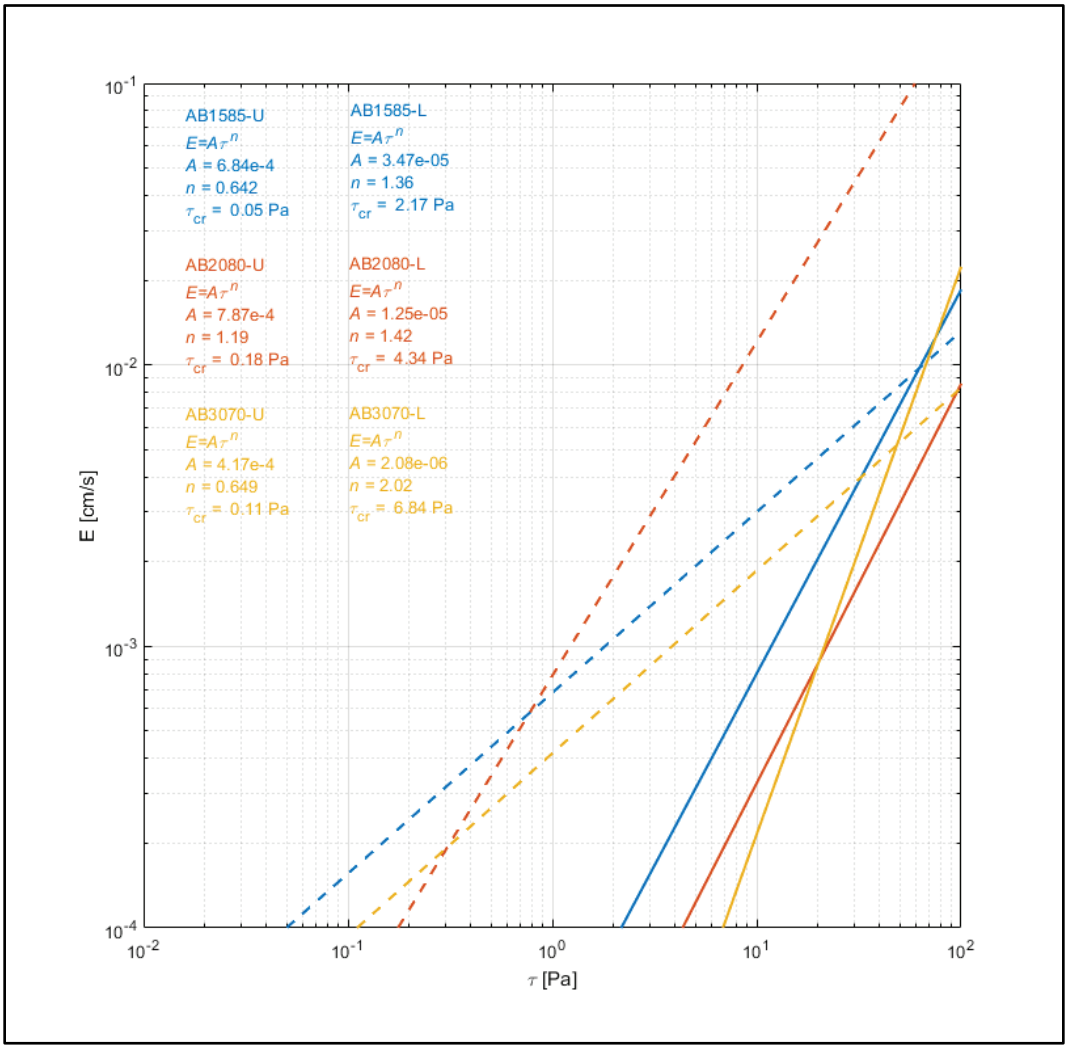

A summary of the erosion parameters is provided in Table 3 separated by upper and lower layers for each AB formulation including the 95% confidence intervals. The large spread in the confidence intervals is attributed to the lack of observations at lower shear stresses and the variability in measured erosion rates.

Table 3. Summary of erosion parameters and associated statistics. Upper layer refers to core depths from 0 to 5 cm, while the lower layer refers to core depths below 5 cm. The merged values in the upper layer were obtained from the model fit of all data points between 0 to cm depth.

Core ID	τ_{cr} (Pa)	τ_{cr}95% Lower	τ_{cr}95% Upper	A	A 95% Lower	A 95% Upper	n	R^2	N
Upper layer									
AB-1585	0.05	0.01	0.19	6.84E-04	2.88E-04	1.62E-03	0.64	0.93	4
AB-2080	0.18	0.06	0.48	7.87E-04	2.04E-04	2.58E-03	1.19	0.92	4
AB-3070	0.11	0.08	0.15	4.17E-04	3.44E-04	5.06E-04	0.65	0.98	6
Merged	0.11	0.08	0.16	5.10E-04	3.84E-04	6.78E-04	0.74	0.84	14
Lower layer									
AB-1585	2.17	0.88	5.34	3.47E-05	1.02E-05	1.18E-04	1.36	0.81	13
AB-2080	4.34	2.25	8.36	1.25E-05	4.92E-05	3.17E-05	1.42	0.89	13
AB-3070	6.84	4.15	11.27	2.08E-06	2.08E-05	7.06E-07	2.02	0.92	16

3.2 Compacted cores

The compacted cores were expected to be extremely erosion resistant. As a result, the cores were eroded at the maximum shear stress of 24 Pa (flow velocity of 4.1 m/s, or 13.1 ft/s) and left to run for multiple hours. For example, the total erosion time for AB-1585 was 190 min over a single day. Likewise, the total erosion time for the WB core was 405 min over 2 days—350 min on day 1 and 55 min on day 2. Consequently, the test results described herein are qualitative since no relationship between erosion rate and shear stress could be established because observations were made at a single (maximum) shear stress.

3.2.1 X-Ray Attenuation (XRA)-derived bulk density

The density scans for the compacted cores are provided in Figure 17. The density of the AB-1585 formulation was variable with values ranging from 1.9 to 2.4 g/cm^3. This variability was likely due to void spaces and variability in the clay-aggregate framework. Likewise, a lower density layer was visible at 30–40 mm depth. This could be attributed to a discontinuity between lifts during core creation. In contrast, the density of the WB core was remarkably consistent with little variability and averaged 1.9 g/cm^3.

Figure 17. XRA-derived bulk density profiles for compacted cores AB-1585 (left) and WB soil (right).

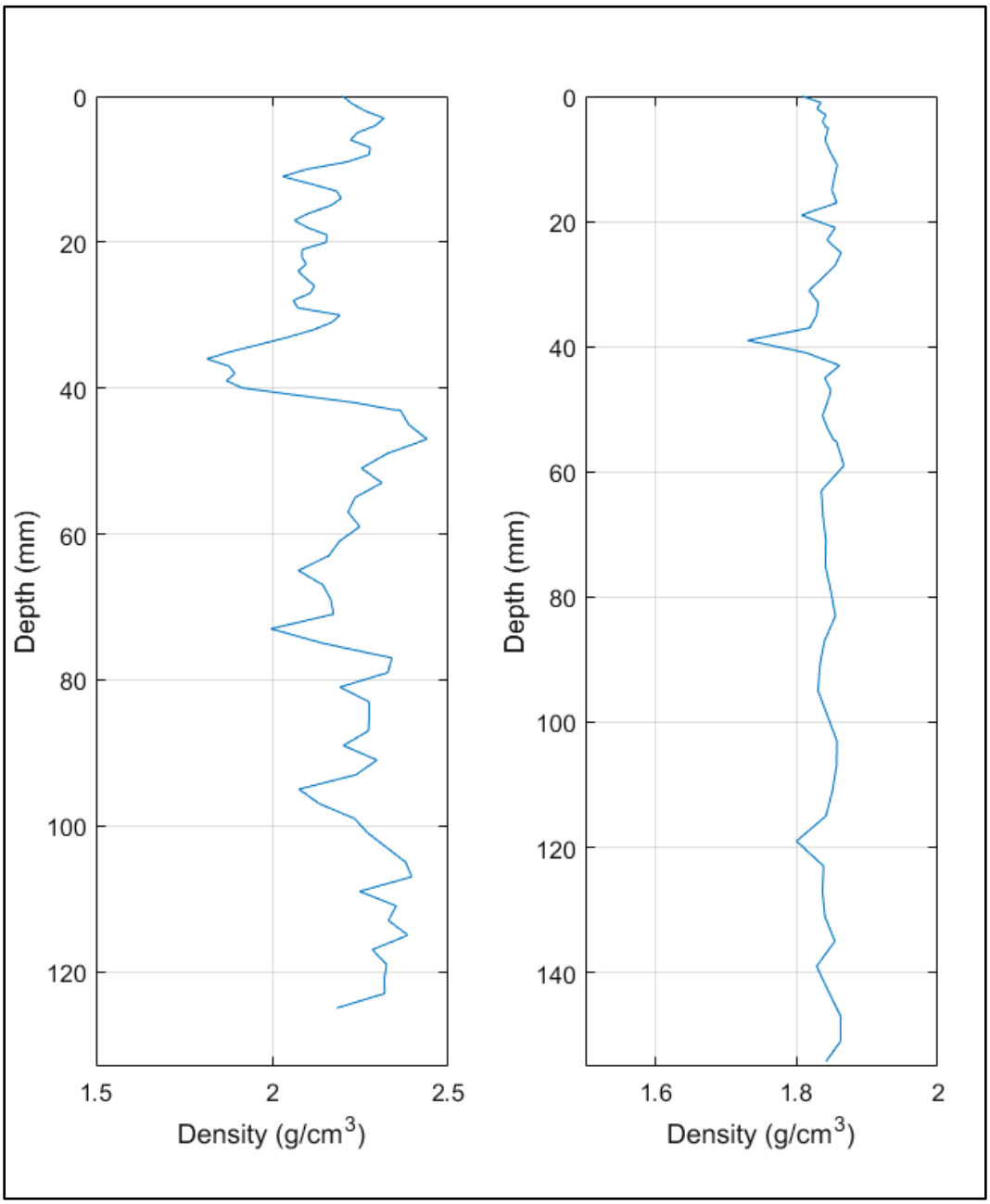

3.2.2 Erosion test results

3.2.2.1 AB-1585

The total, measurable erosion of the compacted AB-1585 formulation was approximately 1.8 cm over a 190 min duration, or an average rate of approximately 5.7 mm/hr under a continuous shear stress of 24 Pa. A sequence of images depicting the core surface in time is presented in

Figure 18. The initial erosion surface was comprised of small, pulverized rock fragments and was relatively planar with only the sides protruding slightly into the flow (Figure 18, 0 min). Most of the small fragments winnowed out within 50 to 60 min into the test leaving behind a surface of exposed gravel. The clay matrix was not readily visible at the surface, implying that cohesive bonding of the gravel aggregate was restricted to the underside of the particles. The winnowing of surface granules and clay matrix increased the surface roughness and undoubtedly turbulent fluid forces. For the remainder of the test, surface erosion persisted as the intermittent plucking of gravel and granules as the surrounding clay matrix eroded. This mechanism of erosion by dislodgement depends on the particle surface area exposed to flow, magnitude of the fluid force, and the cohesive strength of the clay matrix. Since cohesive strength is significantly influenced by water content, the clay matrix continually weakens while exposed to water during the test. Therefore, the erosion behavior over these observation times reflects erosion due to fluid shear stress under a continually changing material state, and thus it is important to note that the measured erosion rates may not accurately predict the physical stability of AB.

Figure 18. Time sequence of erosion for mechanically compacted AB-1585. Total erosion was approximately 1.8 cm over 190 min.

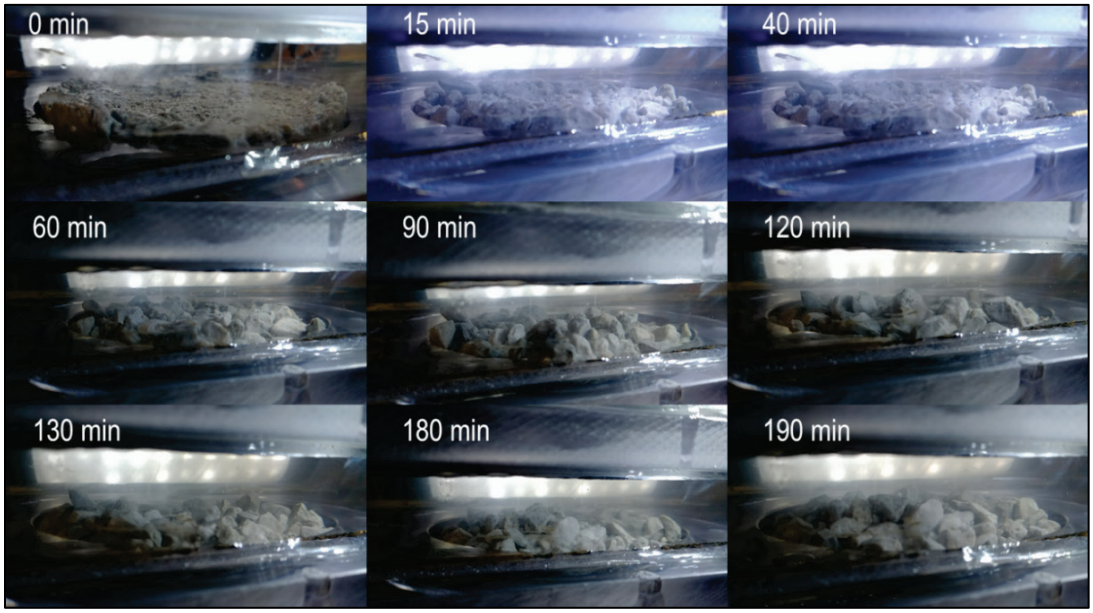

3.2.2.2 WB soil

The measurable erosion of the WB soil was approximately 0.1 cm over a 180 min duration, or an average rate of approximately 0.3 mm/hr under a

maximal, continuous shear stress of 24 Pa. A sequence of images depicting the core surface in time is presented in Figure 19. Initially, the surface was planar and was moderately smooth (0 min). At the maximum shear stress (24 Pa), the surface eroded as small aggregates, leaving behind small divots that increased the surface roughness slightly. Between 0 min and 60 min, it was observed that the surface roughness progressively increased, which indicated that erosion was occurring, yet not at a rate that could be measured easily in Sedflume over these time scales. Consequently, the measurable erosion rate was effectively zero over this duration. After approximately 60 min, the experiment was paused, and the core was left within the Sedflume with overlying water for 120 min. Upon return, it was observed that the core surface had visibly swollen by an estimated 1.0 – 1.5 mm (Figure 19, 120 min). When flow resumed, small mud aggregates were able to erode from the surface under flow conditions as low as 1.0 Pa (20 gpm) indicating the surface had weakened due to water absorption. Again, however, the erosion rate could not be resolved. Therefore, flow was resumed to its maximum after which erosion was initially more aggressive, but then abruptly decreased shortly after. Erosion behavior slowed thereafter to occasional small to medium aggregate erosion during the following 30 min (90 min total erosion time).

Figure 19. Time sequence of erosion for compacted WB soil. Total erosion time is estimated between 0.1 cm to 0.4 cm over 180 min.

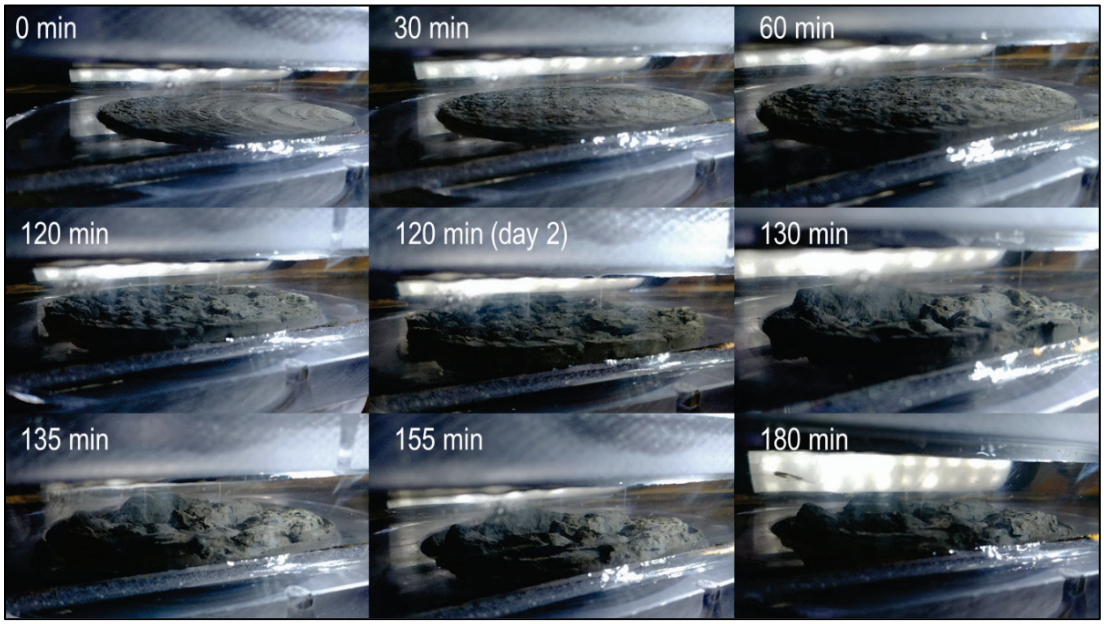

The test continued for another 30 min without significant changes to the core surface or erosion rates (Figure 19, 120 min). The test was then paused at the end of the workday and resumed the following morning. Thus, the total erosion time for day 1 was approximately 120 min. The following morning, and prior to testing, the core surface was again visibly swollen (~ 3 mm) due to absorption of overlying water; the surface was easily erodible with a shear stress of 0.1-0.2 Pa (Figure 19, day 2, 120 min). Upon resuming to the maximum shear stress, the surface eroded as large to very large aggregates, which significantly altered the surface roughness (Figure 19, 130 min). Between 130 to 135 minutes, the erosion behavior initially occurred as intermittent large aggregates then slowed to occasional large aggregates until the experiment was terminated, a total erosion time of 180 min. Considering the uncertainties related to core position, and surface position due to bed roughness changes and surface swelling, the upper limit of erosion is estimated as 3–4 mm over a span of 180 min, which gives an erosion rate of 1.0–1.3 mm/hr with an applied shear stress of 24 Pa. This is approximately the same erosion rate as the non-compacted AB-1585 at 1 Pa applied shear stress.

4 Discussion

4.1 Non-compacted cores

The critical shear stress of the AB upper layers ranged from 0.05 to 0.18 Pa, which is comparable to the critical shear stress of fine silt to fine sand based on the initiation of motion for non-cohesive particles:

$$\tau_{cr} = \theta^*(SG - 1)\rho_w g D \tag{5}$$

where

θ^* = Shields parameter = $\frac{\tau_{cr}}{g(\rho_s - \rho_w)D}$ [–]
SG = specific gravity of the particles [—]
ρ_w = water density [kg/m^3]
ρ_s = particle density [kg/m^3]
g = gravitational acceleration [m/s^2]
D = particle diameter [m].

The critical shear stress of the upper layers did not increase monotonically with increasing clay percentages as was observed with the lower layers. In this sense, the erosion rate parameter derived from the merged data is of the same order of magnitude as that derived separately for the upper layer of each formulation ($A \approx 10^{-4}$). This implies that erosion rates of well-hydrated AB might be independent of clay percentage (or at least the range used in these tests). Combining these data resulted in a reasonable trend to characterize its erosion behavior (r^2=0.84;n=14). However, caution is warranted not to over interpret these results because of the lack of data points. Additional tests would need to be conducted to thoroughly characterize the erosion behavior of fully hydrated AB formulations. Nonetheless, the more hydrated upper layer (< 10 cm core depth) of each AB formulation was found to be significantly more erodible than the underlying material.

The critical shear stresses derived from the lower layers were significantly higher (and erosion rates significantly lower) than the more hydrated upper layers. For the lower layer of each AB formulation, the critical shear

stress increased with increasing clay percentage from approximately 2, to 4, to 7 Pa for AB-1585, AB-2080, and AB-3070, respectively.

While the critical shear stress provides an indication of the threshold for erosion, predicted erosion rates for an applied stress are sensitive to the erosion parameters A and n. Lower values decrease the line slope in the relation of E versus τ_{cr} and indicate an increase in the shear strength of the material. Results from the data analysis showed that A was at least one order of magnitude less for AB-1585 and AB-2080 and two orders of magnitude less for AB-3070, compared to the upper layers, which equates to a reduction in predicted erosion rates by one and two orders of magnitude. These differences can be attributed largely to increases in bulk density and clay percentage.

To place the critical shear stress results into a hydrodynamic context, consider a river system with water depth h. Using the relationship for bed shear stress ($\tau = \rho u_*^2$) and the Karman-Prandtl law of the wall (near-bed velocity profile), a relationship was derived (see Appendix B) to estimate depth-averaged velocities from skin friction shear stress or the shear stress associated with erosion:

$$\bar{u} = \sqrt{\frac{\tau_s}{\rho}} \left(\frac{\ln\left(\frac{h}{z_{ot}e}\right) \ln\left(\frac{z_1}{z_{0s}}\right)}{\kappa \ln\left(\frac{z_1}{z_{0t}}\right)} \right) \tag{6}$$

where

$\bar{u}$ = depth average velocity [m/s]
τ_s = skin friction shear stress [N/m3]
h = water depth [m]
ρ = water density [kg/m3]
z_{ot} = total hydraulic roughness [m]
z_{0s} = skin friction roughness [m]
z_1 = height of near bed velocity above sediment bed [m]
κ = von Karman's constant = 0.4.

Equation 6 estimates mean water velocities using simplifying assumptions. Thus, the relationship is intended only for scale comparisons and not exact predictions. It can be used to provide an idea of velocities

associated with the critical shear stress of erosion for the materials tested (e.g., let τ_{cr} (Table 3)= τ_s). Using Equation 6 applied with h=15 m, z_{0t}=3 × 10^{-3} m, $z_{0s} = \frac{d_{50}}{12}$ =9.2 × 10^{-4} m, and z_1=0.5 m, the depth-averaged water velocities associated with the critical shear stress estimates were calculated as 1.1, 1.5, and 1.9 m/s for AB-1585, AB-2080, and AB-3070, respectively. However, the upper layer, which had an average τ_c=0.11 Pa, would begin to erode at a velocity of 0.2 m/s using the same parameters.

The mass erosion rate per unit area per unit time can be calculated using,

$$E_{mass} = \frac{\rho_b V}{At} \tag{7}$$

where ρ_b is the bulk density, $V = \pi r^2 d$ is the eroded volume where d is the total erosion depth, A=core surface area (inner diameter = 9.75 cm), and t is the total erosion time.

4.1.1 Factors affecting erosion resistance

The performance of AB can be evaluated in primarily two ways: (1) resistance to permeability and (2) resistance to erosion due to hydrodynamic stresses. While much of the published literature on AB performance focused on the former, the present study was meant to address the latter.

The major factors that influence cohesive sediment erosion rates are bed density, particle size, mineral composition, organic content, salinity, and gas content. Other factors include water chemistry and temperature, sodium absorption ratio, and bed roughness, among others. These factors play a significant role in the mechanical properties of cohesive sediment, some of which are further discussed below.

The critical shear stress and erosion rates of cohesive sediments has been found to be particularly sensitive to bed density (Thorn and Parsons 1980; Nicholson and O'Connor 1986; Jepsen et al. 1997). For example, Jepsen et al. (1997) found that erosion rates of cohesive, remolded (laboratory mixed) sediments decreased rapidly with bed density described by this relationship:

$$E = A\tau^n \rho^m \tag{8}$$

where E is the erosion rate (cm/s), τ is shear stress (dynes/cm^2), ρ is bulk density (g/cm^3), and m, n, and A are experimentally determined constants. However, by examining numerous data sets of sand-mud mixtures, Wu et al. (2017) theorized that the mud dry density, and not the mixture dry density, was a key factor affecting critical shear stress.

The influence of water content (and by extension bulk density) on the observed erosion mechanisms can be considered from a soil-mechanical perspective. Winterwerp et al. (2012), for example, demonstrated that the yield strength (the required stress to initiate plastic deformation) of mud is a non-linear function bulk density. They found that the measured strength of various mud samples increased nearly three orders of magnitude with increased bulk density from 1.1 to 1.6 g/cm^3. They additionally found a power law relation between τ_{cr} and the Atterberg Plasticity Index (the range of water content that a cohesive soil behaves plastically), which depends on the clay mineral type, clay content, and water content. Therefore, as a cohesive soil approaches its liquid limit, the yield stress is minimized.

Clay mineralogy and percent clay content can have a marked effect on sediment cohesiveness and erosion resistance. Swelling clays, such as those in the smectite family (e.g., montmorillonite) are inherently more cohesive than those such as illite or kaolinite (the non-swelling clays) due to differences in their crystallographic structures. The differences can be seen indirectly, for example, through measures of cation exchange capacity (CEC) or sodium absorption ratio, and directly using Atterberg Limits. A soil's plasticity index is likewise related to CEC, as those with high CEC also tend to behave more plastically. The effect of percent clay content on erosion resistance was demonstrated through a series of laboratory experiments on sand-mud mixtures (Smith et al. 2015; Perkey et al. 2020). For example, they found that the maximum critical stress of sand-mud mixtures was obtained when mud contents reached 30%–40%, beyond which the critical stress decreased. The decrease is thought to occur once the mud percentage exceeds the pore volume of sand, which changes the sediment framework from grain-supported (connected aggregate boundaries) to matrix-supported (aggregates suspended in a mud matrix).

Jepsen et al. (2000) investigated the effects of gas generation on erosion rates for natural and remolded sediments. Their experiments found that for remolded sediments, the presence of gas decreased bulk densities by up to 10% and increased erosion rates up to a factor of 60.

While the evaluation of permeability was not a focus of this work, understanding the controls on water absorption and transmission through clay materials can elucidate the relation between the water content and material strength. The hydraulic permeability of clay depends in part on clay type and bulk density (along with fluid viscosity) and has been experimentally determined by Pusch (1980a,b) to be on the order of 10^{-12} to 10^{-14} m/s for bulk densities between 1.5 to 1.9 g/cm^3, respectively. The permeability of AB (specific formulation not reported) was measured to be on the order of 10^{-9} to 10^{-8} m/s (Barth et al. 2008). However, the rate of hydration depends on the electrochemical properties of the clay (for example, matric (capillary) and osmotic potential) and loading pressure (Shirazi et al. 2010). Thus, the hydration (or swelling) rate is initially fast then slows as water potential is decreased; thereafter, the permeability decreases abruptly (Shirazi et al. 2010). This process may explain the trends of bulk densities observed in the AB cores. The reason is that during core construction, successive material lifts reduces water availability due to displacement of overlying water, while the swelling of the clays reduces permeability. Further swelling is prevented by additional overburden (from subsequent AB lifts) and the confining boundaries of the core tube. The confined swelling behavior related to the reduction of in-situ water is made evident by the lack of pore-filling behavior below about 5 cm depth (see Figure 7). The final lift, however, which had several centimeters of overlying water, had virtually an inexhaustible supply of water to hydrate. The core surface was exposed to overlying water for approximately 24 hours between core creation and x-ray scanning. Consequently, hydration of the AB clay matrix reduced bulk densities from approximately 1.6–1.7 g/cm^3 below 10 cm to approximately 1.2 g/cm^3 near the surface with a gradual transition in between (Figure 8). The obvious conclusion is that the rheological properties of the AB clay matrix changes rapidly under continuous exposure to water which greatly influences erosion resistance. Consequently, erosion rates derived from Sedflume might have been different depending on the choice of time intervals used for the aggregate lifts during core construction, and this aspect should be taken into consideration in future capping designs.

4.1.2 Comparison of AB erosion resistance to previous work

The critical shear stress results obtained from the present study can be compared to those from the US EPA capping demonstration project in 2006 described in the Introduction of this report. For that purpose, additional details are warranted here. The EPA SITE project was a field trial designed

to evaluate different capping technologies, the primary functions of which were to stabilize the sediment substrate and prevent contaminant transport into the water column. In that study, four cores were collected within test quadrants along the Anacostia River at 6 months and 30 months post application. Two quadrants had either an AB-based cap or a sand-only cap to compare to a control quadrant with no cap. The cores were eroded in a Sedflume apparatus operated by Sea Engineering, Inc. The AB material used in the field trial was smaller (mean of 3.5 mm with 10% of the particles > 2 mm) compared to the current study (9–3 mm). Additionally, the retrieved cores generally had 5–10 cm of sand or silt overburden above the AB material (ranging 15–50 cm thick), which was typically interspersed near the top and bottom horizons of the AB layer. The reported average bulk density of the AB material was 1.33 g/cm^3 and ranged from 1.16 to 1.60 g/cm^3.

In the final US EPA report (US EPA 2007), the critical shear stress of the AB cores was reported to range from 3.2 to 10 Pa, although the upper value appears to be overstated. Upon examining the data provided in the appendices, it is evident that while the applied shear stresses used in the erosion tests often reached 10 Pa, typically there were only 2 or 3 data points (Figure 20) within the pure AB layer (i.e., not affected by sediment transitions from the top and bottom horizons). Therefore, the critical stress for erosion of 10 Pa is based on ad hoc reasoning and not the model fit of Equation 1. The standard Sedflume test procedure at that time was to double the applied stress from a small initial value to a maximum, then revisit those stresses in a series of erosion cycles—for the US EPA field trial, this ranged from 0.1 to 6.4 Pa, and then finally 10 Pa (the limit of that particular Sedflume apparatus). The graphs of erosion rate versus depth for the cores taken at 6 months showed that once the AB layer was encountered, erosion rates usually could only be measured using shear stresses of 6.4 Pa and 10 Pa (Figure 20). The erosion rates at the next lowest shear stress of 3.2 Pa were effectively zero (or not measureable). For these cores, it implies the critical stress was somewhere closer to 3.2 Pa.

To estimate the critical stress from these data, data point pairs of erosion rate and applied shear stress (confined within the AB layer) were extracted from the graphs and entered into an interpolation function that extrapolated the data to the critical threshold of E = 10^{-4} cm/s. This calculation was possible for three of four cores—the critical shear stresses

obtained were 4.1, 2.8, and 3.6 Pa for mean value of 3.6 Pa. These values were similar to those reported for the cores taken at 30 months, which had a mean of 3.1 Pa and ranged from 2.6 to 3.4 Pa (Table 4).*

Figure 20. Image of core AQ-5 and measured erosion rates with depth, US EPA field experiment 30-month, post-application. The gray bar highlights the data point pair used to estimate the critical shear stress in the AB horizon. Modified from Sea Engineering, Inc. (unpublished data)†.

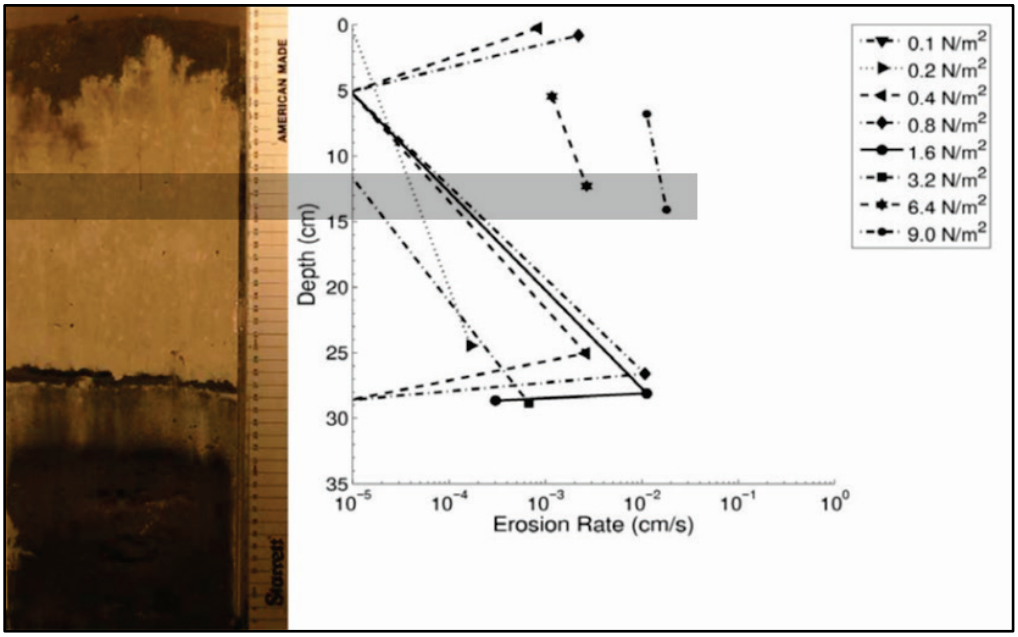

* Note that the reported average values of critical shear stress, bulk density, and particle size tabulated in the appendix of the 30-month report were averaged across multiple and different sedimentary horizons. Thus, the averaged tabulated data have no physical basis for the interpretation of AB erosion resistance and should not be relied upon.

† Sea Engineering, Inc. (SE). 2006. Draft. *Sedflume Analysis of Capping Technologies – 30 Months*, Anacostia River, Washington, DC. December 11, 2006.

Table 4. Erosion results from the US EPA field experiment 6-month (mo.) and 30-month post application.

CORE ID		ρ_b (g/cm^3)	E (cm/s)	τ_b (Pa)	τ_{cr} (Pa) Reported	τ_{cr} (Pa) Estimated
SF-8	Field-6 mo.	1.63	3.0 E-04	6.4	NR	4.3
			1.1 E-03	10	NR	-
SF-9	Field-6 mo.	1.25	9.0 E-04	6.4	NR	2.8
			3.0 E-03	10	NR	-
SF-10	Field-6 mo.	1.32	8.0 E-04	6.4	NR	3.6
			4.0 E-03	10	NR	-
AQ-5	Field-30 mo.	1.24	2.8 E-03	6.4	3.3	-
			2.0 E-02	9	3.5	-
AQ-7	Field-30 mo.	1.41	1.7 E-03	6.4	3.4	-
			1.9 E-02	9	2.1	-
AQ-8	Field-30 mo.	1.29	1.8 E-04	3.2	5.1	-
			3.2 E-04	6.4	3.3	-
			1.9 E-03	9	3.3	-

The critical shear stress of AB-2080 (4.34 Pa) used in this study is higher than the formulation used in the EPA SITE study (3.1–3.6 Pa). The present results also suggest that AB-1585 is less erosion resistant (2.17 Pa) while AB-3070 is more erosion resistant (6.84 Pa) compared to the US EPA formulation, though comparisons of predicted erosion rates should be made in addition to critical shear stress. However, comparisons of predicted erosion rates cannot be made accurately because erosion parameters were not published (or could not be determined) from the US EPA study.

4.1.3 Implications for capping applications

The thickness of AB used as a cap is often limited to a few to several inches to reduce material costs (compared to traditional capping materials such as sand). This is reasoned to be acceptable based on AB having low permeability and presumed high erosion resistance. However, the erosion test results of this study clearly demonstrate that erosion resistance of AB is greatly reduced once the clay is fully hydrated, even at low shear stress. Thus, understanding and predicting the physical stability of AB for performance and life-cycle analysis should consider this potential change in material state.

To illustrate, the longevity of an exposed AB cap should theoretically depend on its bed thickness, the thickness of the overhydrated upper layer, and the number of critical events expected (i.e., those exceeding the critical threshold for erosion) based on a probabilistic recurrence interval, and the duration of those events above the threshold shear stress (Figure 21). For example, suppose an AB-1585 cap in the field is 50 cm thick and sufficiently large in the other two dimensions to ignore edge effects. If the upper 5 cm is hydrated similar to that observed in this study, then the total erosion time can be calculated using the values in Table 3 (AB-1585_upper) as a function of shear stress above the critical stress. In this case, the total time to erode 5 cm is approximately 9 hr at a constant shear stress of 0.1 Pa, or 2 hr at 1 Pa. Assuming that full removal of the upper layer allows another 5 cm to become hydrated to the same gelled state as before, then this simplified analysis would suggest that the AB cap could withstand 10 erosion events at that magnitude and duration. If a 1-Pa event with 2 hr duration had a recurrence interval of 1 year, it would suggest a longevity of approximately 10 years. This simplified exercise is intended to provide order-of-magnitude approximations of a life-cycle analysis. Note that this calculation is for surface erosion only under steady flow conditions and does not consider mass erosion due to form drag, which can greatly accelerate erosion.* Consequently, Equation 1 applies only for surface erosion. The shear stress required to transition from surface erosion to mass erosion varies depending on the bulk properties of the material and surface roughness and cannot be properly determined using Sedflume.

* Briefly, the primary modes of erosion can be simplified as surface erosion and mass erosion. Surface erosion is described as the gradual removal and entrainment of particles related to the strength of surface flocs. Conversely, mass erosion is related to a bulk physical property that is characterized, in part, by the yield strength of the material, whereby relatively large masses can be torn from the bed when subjected to high shear stress (Winterwerp and van Kesteren 2004; Mehta and McAnally 2008; Winterwerp et al. 2012).

Figure 21. Calculated times (in hours) to total erosion of a 5 cm placement of non-compacted AB (1585 freshwater formulation) as a function of bed shear stress exceeding the critical stress. The calculation assumes continuous surface erosion under steady flow conditions. The plot on the left represents a fully hydrated AB-1585 scenario exposed to free water (τ_{cr} = 0.05 Pa) while right plot represents the more resistant layer below (τ_{cr} = 2.17 Pa). Dashed lines represent the spread based on the uncertainty in the critical stress values (Table 2).

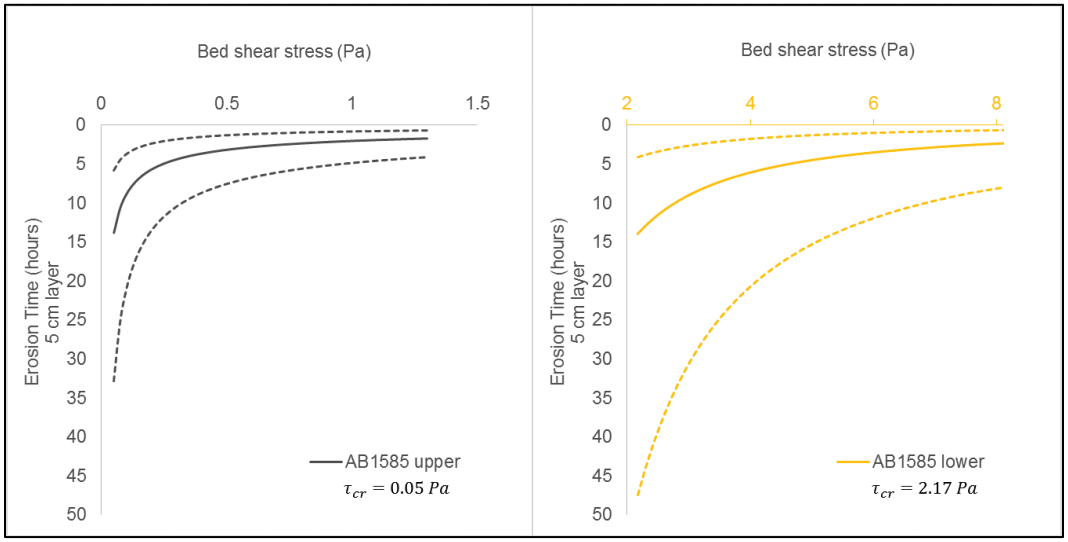

Additionally, under the US Army Corps of Engineers (USACE), Dredging Operations and Environmental Research (DOER) program, and Engineering with Nature (EWN) initiative, applied research is ongoing to cost-effectively maximize dredged fine-grained sediment (FGS) for beneficial use projects. However, the application of dredged FGS is typically limited to non-energetic environments, such as thin-layer placement, since the material is vulnerable to erosion prior to consolidation. Although additional uses for FGS have been proposed, such as the construction of mud berms adjacent to wetland restoration sites to dissipate wave energy, such features are anticipated to have a short life expectancy unless the sediment is amended with a stabilizing agent, such as AB or other material. Therefore, in addition to the capping and levee repair applications, this research will also help evaluate the potential for amending dredged FGS with AB for cost-effective sediment stabilization.

4.2 Compacted cores

The erosion resistance of the AB and a natural soil (WB) were tested while in a highly compacted state. The compacted AB and WB cores each demonstrated high erosion resistance, which is undoubtedly due to their increased bed densities. However, the erosion test results, although

limited, also showed that the WB soil was more erosion resistant—its measured erosion rate was five times less than the AB material despite its lower bulk density. The compacted AB might have been expected to erode less due to its greater bulk density. Though in this case, the greater density is related more to the contribution of the stone particles within the AB composite and not its degree of compaction. Since both materials were compacted with the same mechanical effort at their respective optimal moisture contents, the compaction of AB was limited by the grain-to-grain contacts of the stone aggregate. Therefore, the AB clay matrix is expected to have a lower shear strength than that of the WB soil, which likely affected erosion rates. Other contributions may be attributed to differences in mode of erosion, surface roughness, grain size, and mineral composition as discussed below.

For the WB soil, surface erosion manifested as small to medium bed aggregates and was dominant through most of the testing. The WB soil was also observed to erode by mass erosion, though these events were limited and occurred only after a 2 hr delay in erosion testing allowed the soil to hydrate and swell to a higher position in the flume channel. Most of the observed erosion occurred this way. Conversely, due to the incorporation of gravel aggregate, the AB material had a persistent bed roughness, which is known to increase erosion susceptibility resulting from larger turbulent fluctuations in water velocity. Furthermore, exposure of the aggregate by winnowing eventually causes erosion by particle detachment, which may carry with it some additional clay material adhered to bottom of the particle. Conceptually, particle detachment should occur when the sum of drag forces around the particle exceeds the resistive cohesive bonding of the particle. From laboratory experiments, Schmeekle et al. (2007) found that the maximum drag on gravel-sized particles that protrude above the bed by half their diameter is as much as four times its mean.

The mass erosion rate per unit area per unit time was calculated using Equation 7 and average bulk densities. Conservatively assuming a total erosion depth of 2 mm over 180 min (since the surface did not erode evenly), the mass erosion rate of WB is estimated as 1.3 kg/m^2/hr when subjected to a shear stress of 24 Pa. This rate is expected to be greater as the upper surface absorbs water and changes it rheology to a weaker state.

4.2.1 Potential use as a levee repair material

A primary motivation for testing compacted AB was to evaluate its potential as a levee repair material compared to that of a natural material such as the WB soil. Testing via Sedflume is useful in assessing erodibility caused by fluid shear stress. As such, these tests are more relevant to AB formulations used in applications like subaqueous sediment caps or sequestration layers. An engineered composite material such as AB has the potential to replace or augment natural soils in levee repair designs, although a proper evaluation is outside the capabilities of Sedflume because of the different erosion mechanisms at work. Nonetheless, it is instructive to look at some potential applications.

There are various causes of erosion that can affect the integrity of a levee that may result in a breach without proper repairs. The two most common causes of level failure are overtopping and internal erosion (Hanson et al. 2010). Other examples include rilling or gullying from rain runoff, erosion by wave attack during high water, and slope failure due to either current scour or soil seepage. Repairs to levee embankments often call for scarifying and backfilling the affected areas using the same material that the levee is made of, or from an acceptable borrow area, which is then mechanically compacted to add strength. In the event of limited access or quantities of cohesive soils, AB could make a reasonable substitute, based on Sedflume erosion results, with some important considerations.

One consideration is that the borrow material should be generally compatible with the embankment soil as there may be inherently weak planes along contact borders. It is well understood that surface discontinuities can initiate erosion and contribute to eventual failure (Powledge et al. 1989). Another is that the borrowed fill material needs to be sufficiently compacted to be effective. Better compaction of AB may achieved if the aggregate used were smaller since inadequate compaction may lead to decreased strength and could allow for seepage paths (USACE 2000). By means of laboratory jet erosion testing, Hanson et al. (2010) showed that soil texture and level of compaction influences the erodibility of embankment soils. Using a device (the Erosion Function Apparatus, or EFA) that operates similarly to Sedflume, Briaud et al. (2008) eroded levee soils subjected to overtopping and found a large variation in their erosion resistances. Numerical simulation results by Briaud et al. (2008) also showed that shear stresses due to overtopping

could be as high as 30–40 Pa on the levee surface and up to 50–60 Pa near the toe of the levee.

Another concern remains regarding AB surface integrity after multiple wet and dry periods post capping. The extreme swelling nature of the bentonite used in the formulations may exacerbate desiccation cracking and erosion by rip-up clasts in subsequent overtopping or sheet flow events. (This effect could be lessened by planting protective vegetation, which has been shown to successfully root within AB substrate*, and the addition of vegetation is known to provide significant overtopping protection and slope stabilization). AB may not be suitable to be used for current scour protection near the toe of the levee where it would be in constant contact with water, owing to the weakening effects upon hydration.

Additional laboratory tests would be necessary to properly evaluate the response of AB to overtopping. One option would be to conduct overtopping tests within a small-scale flume. Based on those results, testing could be scaled up to a physical model basin or a near prototype scale using a unique, ERDC-based facility designed to investigate levee breach repair systems.

4.2.2 Potential use as an embankment dam core material

Certain types of engineered levees (or embankment dams for reservoirs) are often constructed using an impervious core made from a fat (swelling) clay. This design is meant to reduce the probability of failure due to excessive internal erosion by piping. However, another cause of failure is due to differential settlement between the core, which is impermeable but relatively compressible, and the shell, which is permeable but incompressible (Nayebzadeh and Mohammadi 2011). The resulting differential settlement can cause internal forces to be transferred from the core to the shell resulting in tensional fracturing of the core (Nayebzadeh and Mohammadi 2011), which can increase the likelihood of piping. In this case, AB may make a good candidate as a core material since it can be formulated as a mixture of clay and stone aggregate. This would have the advantage of being impermeable while offering structural integrity against compressive (for vertical cores), or both compressive and shear forces (in the case of inclined cores) due to the interlocking nature of the aggregate

* John Hull. Personal communication. July 2019. AquaBlok, Inc.

grain boundaries. One potential concern, however, is the amount of internal pressure created by swelling if AB comes into contact with too much moisture. Here, the overburden pressure of the shell would have to exceed the swelling pressure of the clay. Different formulations using different clay types could be explored for this purpose.

4.3 Considerations for AB formulations

The erosion resistance of sodium bentonite (a high swelling clay predominately used in AB formulations) depends highly on its water content. The full saturation of bentonite clay may be as high as a 10:1 weight ratio of water to clay (Desai et al. 2012). Therefore, the erosion resistance of AB clay might be expected to vary by a wide range depending on the amount of hydration. Freshwater AB contains an abundance of bentonite clays (chiefly sodium montmorillonite) that can absorb large quantities of water, swelling to approximately 5–10 times its original volume. Saltwater AB formulations contain more Attapulgite (chiefly Palygorskite)*, which does not have the same swelling potential as bentonite due to its crystalline structure. Consequently, the plasticity index of Attapulgite (~60) is much lower than sodium bentonite, which can reach plasticity index values exceeding 600.

In general, the erosion resistance of AB formulations is due to a combination of the cohesiveness and bulk density of the clay matrix and the size distribution and packing arrangement of its composite gravel. The maximum critical shear stress at the optimum mud content was approximately one order of magnitude greater than that of fine sand ($\tau_{cr\_sand} \cong 0.17$) and corresponded to the minima of erosion rates. Therefore, AB formulations may be optimized by adjusting the clay percentage to the pore volume of the aggregate used and using well-graded gravel. This strategy is intended to add strength to the material by maximizing grain-on-grain contact after hydration and consolidation.

Finally, the use of a polymer treatment may act to reduce the cohesive strength of AB. Treating bentonite with a polymer has been reported to increase the separation of clay platelets, which increases hydration potential (CETCO 2013). A stated benefit of such a treatment is to enhance

* John Hull. Personal communication. July 2019. AquaBlok, Inc.

chemical containment by reducing permeability but perhaps at the expense of lowered erosion resistance by encouraging hydration.

5 Conclusions and Recommendations

New formulations of AB that use larger gravel mixed with varying percentages of clay (15%, 20%, and 30% clay by weight) were tested for erosion resistance in non-compacted and compacted states using Sedflume. Tests in the non-compacted state were meant to simulate erosion resistance for subaqueous capping applications. The erosion resistance of compacted AB was compared to a natural soil with high plasticity and compacted using the same mechanical effort. These tests were meant to simulate the compacted state of levee repair soils and their erosion resistance against high velocity flows from levee overtopping events.

Erosion results of the non-compacted AB showed that erodibility was dependent on the bulk density (and thus water content) of the AB formulation. The swelling, pore-filling nature of hydrated bentonite may excel at reducing permeability, though at the expense of decreased erosion resistance. The reason for this result is two-fold: (1) the pore-filling behavior of the clays can change the sediment framework from clast-supported to matrix-supported, and therefore does not benefit from the added stability of grain-on-grain contacts and (2) the large capacity of swelling clays to absorb water decreases the bulk density and therefore the cohesive yield strength of the material. The depth of hydration, and thus the extent of this weakened layer, largely depends on the availability of surrounding water (i.e., pore water becomes limited whereas water above the sediment-water interface is unlimited). Since bentonite is also impermeable, this effect was limited to the upper 5–10 cm in laboratory tests. However, the non-linear hydration rate may have implications for time intervals used between successive product applications in the field. Understanding the balance between these processes will lead to optimized permeability and erosion resistance. Furthermore, the hydrated layer and its extent should be considered in capping designs and life-cycle analyses. Therefore, the average critical shear stress of the hydrated upper layers was 20–60 times less than the non-hydrated layers depending on the formulation. There were no significant differences in critical shear stress or erosion rate parameter between the hydrated upper layers regardless of clay content.

The increase in bulk densities from 1.0 to 1.5 g/cm^3 above 5 cm depth to 1.6–1.7 g/cm^3 below 5–6 cm showed a marked difference in erosion resistance for each formulation. In this case, the critical stress increased, and predicted erosion rates decreased with increasing clay content in the AB

formulations; however, hydration of the clay over time must be considered with this result. Additionally, increasing the clay content beyond the porosity of the composite used will likely not result in more erosion resistance based on previous work, which has shown erosion resistance is maximized when clay percentage approaches the porosity of the sediment framework, then decreases thereafter (Smith et al. 2015; Perkey et al. 2020). Further erosion studies should include (1) quantifying erosion parameters using AB formulations with different clay types or mixtures under grain-supported and matrix-supported frameworks, (2) quantifying erosion resistance relative to clay hydration rate and extent in relation to clay type, (3) evaluating erosion resistance under different product application scenarios and overburden thicknesses, and (4) evaluating the erosion resistance of AB-amended dredged sediments.

The compacted AB and WB soil both demonstrated high erosion resistance. However, the results are qualitative since critical stresses and erosion parameters could not be established due to limited data. The WB soil was slightly more erosion resistant, but this was likely due to (1) a denser, more compacted state and (2) lower surface roughness and drag forces across grain boundaries. Therefore, the performance of AB used for overtopping protection may be improved if the sizes of the aggregates were reduced. However, further Sedflume tests would need to be conducted for validation. Additionally, erosion from overtopping is more complex and can be initiated by numerous mechanisms that cannot be investigated using Sedflume. Thus, flume experiments and near-prototype scale models should be explored to gauge AB erosion by other failure mechanisms. In contrast, the combination of low permeability and structural integrity of a clast-supported formulation could make an excellent alternative as a dam core to protect against differential settling by strain. This is a line of research that should be explored using near-prototype scale models.

Additionally, under the USACE DOER program and EWN initiative, applied research is ongoing to cost-effectively maximize dredged FGS for beneficial use projects. However, the application of dredged FGS is typically limited to non-energetic environments, such as thin-layer placement, since the material is vulnerable to erosion prior to consolidation. Although, additional uses for FGS have been proposed, such as the construction of mud berms adjacent to wetland restoration sites to dissipate wave energy. Such features are anticipated to be very dynamic and have a short life expectancy unless the sediment is amended with a stabilizing agent, such as

AB or other material. Therefore, in addition to the capping and levee repair applications, this and future research will help evaluate the potential for amending dredged FGS with AB for cost-effective sediment stabilization.

References

Akahori, Ryosuke, Mark W. Schmeeckle, David J. Topping, and Theodore S. Melis. 2008. "Erosion Properties of Cohesive Sediments in the Colorado River in Grand Canyon." *River Research and Applications* 24: 1160–1174. https://doi.org/10.1002/rra.1122

ASTM Standard D698. 2012. *Standard Test Methods for Laboratory Compaction Characteristics of Soil Using Standard Effort*. West Conshohocken, PA: ASTM International.

Barth, Edwin F., Danny Reible, and Andrew Bullard. 2008. "Evaluation of the Physical Stability, Groundwater Seepage Control, and Faunal Changes Associated with an AquaBlok Sediment Cap." *Remediation* 18(4): 63–70. DOI: 10.1002/rem.20183

Been, Kenneth 1981. "Nondestructive Soil Bulk Density Measurements by X-ray Attenuation." *Geotechnical Testing Journal* 4(4): 169–176.

Briaud, J. L., H. C. Chen, A. V. Govindasamy, and R. Storesund. 2008. "Levee Erosion by Overtopping in New Orleans during the Katrina Hurricane." *Journal of Geotechnical and Geoenvironmental Engineering* 134(5): 618–632. DOI: 10.1061/(ASCE)1090-0241(2008)134:5(618)

CETCO. 2013. *Sodium Bentonite: Its Structure and Properties*. Technical Reference GN-001.

Desai, Reshma R., J. A. Erwin Desa, and V. K. Aswal. 2012. "Hydration Studies of Bentonite Clay." *Conference Proceedings of the American Institute of Physics* 1447, 197. DOI: 10.1063/1.4709948

Jepsen, R., J. Roberts, and W. Lick. 1997. "Effects of Bulk Density on Sediment Erosion Rates." *Water, Air, and Soil Pollution* 99(21). DOI: 10.1007BF02406841

Jepsen, R., Joe McNeil, and Wilbert Lick. 2000. "Effects of Gas Generation on the Density and Erosion of Sediments from the Grand River." *Journal of Great Lakes Research* 26(2): 209–219. DOI: 10.1016/S0380-133-(00)70687-3

Hanson, Gregory J., Tony Wahl, Darrel Temple, Sherry Hunt, and Ron Tejral. 2010. "Erodibility Characteristics of Embankment Materials." *Conference Proceedings, Association of State Dam Safety, Seattle, WA*.

Hull, John, J. M. Jersak, and C. A. Kasper1999. "In Situ Capping of Contaminated Sediments: Comparing the Relative Effectiveness of Sand Versus Clay Mineral Sediment Caps." *In Proceedings of the 1999 Conference on Hazardous Waste Research, St. Louis, MO, pp. 286-311.*

Lick, W., J. Lick, L. Jin, and J. Gailani. 2007. "Approximate Equations for Sediment Erosion Rates." *Proceedings in Marine Science*. Edited by J.P.-Y Maa, L. P. Sanford, and D. H. Schoellhamer. *Estuarine and Coastal Fine Sediments Dynamics* 8. DOI: 10.1016/S1568-2692(07)80009-X

McNeil, J., C. Taylor, and W. Lick, 1996. "Measurements of Erosion of Undisturbed Bottom Sediments with Depth." *Journal of Hydraulic Engineering* 122(6); 316–324.

Mehta, A. J., and W. H. McAnally. 2008. "Fine Grained Sediment Transport." *Sedimentation Engineering: Processes, Measurements, Modeling, and Practice*. MOP110. DOI: 10.1061/9780784408148.ch04

National Watershed Conference. 2001. National Watershed Coalition, Richmond, VA, May 21–23, 2001.

Nayebzadeh, R., and Mohammadi, M. 2011. "The Effect of Impervious Clay Core Shape on the Stability of Embankment Dams." *Geotechnical and Geological Engineering* 29: 627–637. DOI: 10.1007/s10706-011-9395-z

Nicholson, J., and B. A. O'Connor. 1986. "Cohesive Sediment Transport Model." *Journal of Hydraulic Engineering* 112(7): 621–640.

Palermo, M. R., S. Maynord, J. Miller, and D. Reible. 1998. *Guidance for In Situ Subaqueous Capping of Contaminated Sediments*. EPA 905-B96-004. Chicago, IL: Great Lakes National Program Office.

Perkey, David W., S. Jarrell Smith, and A.M. Priestas. 2020. *Erosion Thresholds and Rates for Sand-Mud Mixtures*. ERDC-CHL TR-20-13. Vicksburg, MS: US Army Engineer Research and Development Center.

Powledge, George R., David C. Ralston, Paul Miller, Yung Hai Chen, Paul E. Clopper, and D. M. Temple. 1989. "Mechanics of Overflow Erosion on Embankments. I: Research Activities." *Journal of Hydraulic Engineering* 115(8): 1040–1055.

Pusch, R. 1980a. *Permeability of Highly Compacted Bentonite*. SKBF/KBS Technical Report 12-23. Division Soil Mechanics, University of Luleå.

Pusch, R. 1980b. *Water Uptake, Migration, and Swelling Characteristics of Unsaturated and Saturated Highly Compacted Bentonite*. SKBF/KBS Technical Report 80-11. Division Soil Mechanics, University of Luleå.

Roberts, J., R. Jepsen, D. Gotthard, and W. Lick. 1998. "Effects of Particle Size and Bulk Density on Erosion of Quartz Particles." *Journal of Hydraulic Engineering* 124: 1261–1267.

Schmeeckle, M. W., J. M. Nelson, and R. L. Shreve. 2007. "Forces on Stationary Particles in Near-Bed Turbulent Flows." *Journal of Geophysical Research* 112: F02003. DOI: 10.1029/2006JF000536

Shirazi, S. M., H. Kazama, F. A. Salman, F. Othman, and S. Akib. 2010. *International Journal of the Physical Sciences* 5 (11): 1647–1659.

Smith, S. J., D. W. Perkey, and A. M. Priestas. 2015. "Erosion Thresholds and Rates for Sand-Mud Mixtures." In *Proceedings of the 13th International Conference on Cohesive Sediment Transport Processes (INTERCOH), Leuven, Belgium*, 7–11.

Thorn, M. F. C., and J. G. Parsons. 1980. "Erosion of Cohesive Sediments in Estuaries: An Engineering Guide." *Third International Symposium of Dredging Technology* Bordeaux, 349-358. BHRA, Cranfield. http://www.worldcat.org/oclc/839373128

USACE (US Army Corps of Engineers). 2000. *Design and Construction of Levees*. EM 1110-2-1913. Washington, DC.

US EPA (US Environmental Protection Agency). 2007. *Demonstration of the AquaBlok Sediment Capping Technology*. Innovative Technology Evaluation Final Report. EPA/540/R-07/008. Washington, DC.

Winterwerp, J. C., and W. G. M. Van Kesteren. 2004. "Introduction to the Physics of Cohesive Sediment in the Marine Environment." *Developments in Sedimentology*. Volume 56. Elsevier ISBN:0-4444-51553-4.

Winterwerp, J. C., W. G. M. van Kesteren, B. van Prooijen, and W. Jacobs. 2012. "A Conceptual Framework for Shear Flow-Induced Erosion of Soft Cohesive Sediment Beds." *Journal of Geophysical Research* 117: C10020. DOI: 10.1029/2012JC008072

Wu, W., C. Perera, S. J. Smith, and A. Sanchez. 2017. "Critical Shear Stress for Erosion of Sand and Mud Mixtures." *Journal of Hydraulic Research* 56(1): 96–110. DOI: 10.1080/00221686.2017.1300195

Appendix A: Description of XRA-derived Bulk Density

The XRA device produces non-destructive bulk density measurements with high vertical spatial resolution (up to 1 mm) and high accuracy. The X-rays are generated using a 160 kV Gulmay X-ray tube with a tungsten target and collimated to a narrow 1 mm beam that penetrates the sample. The transmitted energy through the sample is detected as a count rate using an Amptek XR-100CR X-ray detector. The attenuation of radiation through a material is dependent on the density and thickness of the absorbing material and can be described by the well-known Beer-Lambert Law (Equation A-1):

$$I = I_0 \exp(-\mu \rho x) \tag{A-1}$$

where

I = transmitted radiation intensity
I_o = incident radiation energy
μ = mass attenuation coefficient
ρ = material density
x = material thickness.

The incident and transmitted radiation intensities can be expressed as the number of photons generated and detected as counts per second. Thus, Equation A-1 can be expressed as follows (Been 1981):

$$N = N_0 \exp(-\mu \rho_b d) \tag{A-2}$$

where

N = count rate with sample
N_o = count rate of a reference material
μ = mass attenuation coefficient
P_b = material bulk density
d = sample diameter.

Rearranging Equation 2 for material bulk density gives the following:

$$\rho_b = -\frac{1}{\mu d}\ln\left(\frac{N_0}{N}\right) \quad \text{(A-3)}$$

where the parameters N, N_0, and d are measured and the mass attenuation coefficient is determined through a series of calibrations. To account for the effects of the polycarbonate wall and any change in temperature that may occur during the density scan, calibrations (I_0 reference scans) are performed periodically (and automatically) by scanning a short polycarbonate tube filled only with distilled water (used as the reference material).

The variance in density estimates decreases with the total number of counts detected and therefore the scan time. Scan times were set for 30 sec, which generated more than 300,000 counts per measurement. Based on calibrations using a known reference material, the relative error at this count rate was determined to be better than ±0.01 g/cm^3 at the 95% confidence level.

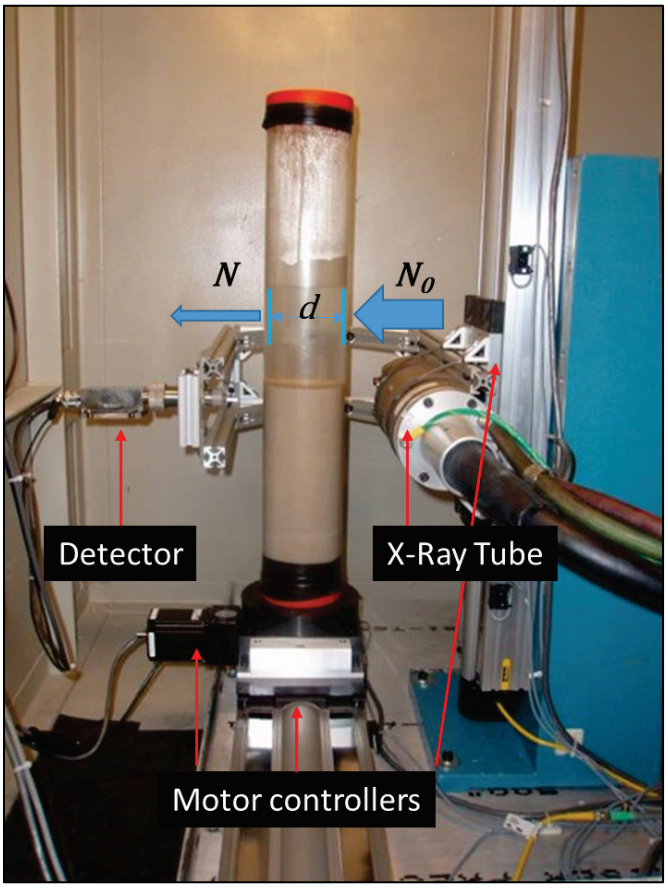

Appendix B: Derivation of Depth to Apply Depth-Averaged Velocity in a Log-Velocity Distribution

The following language and derivation was written and supplied by S. Jarrell Smith*.

In applications where depth-averaged velocities are used to compute bed stress, it is often useful to use the logarithmic boundary layer assumption for estimating the shear velocity, u_*, and bed shear, τ_b. The following derivation determines the appropriate height above the sediment bed, z, and gives equations for directly estimating u_* and τ_b from depth-averaged velocities.

The expression for logarithmic vertical distribution of velocities (law of the wall) is

$$u(z) = \frac{u_*}{\kappa} \ln\left(\frac{z}{z_0}\right) \tag{B-1}$$

And the depth-averaged velocity is

$$\bar{u} = \frac{\int_{z_0}^{h} \frac{u_*}{\kappa} \ln\left(\frac{z}{z_0}\right) dz}{\int_{z_0}^{h} z\, dz} = \frac{\frac{u_*}{\kappa} \int_{z_0}^{h} \ln\left(\frac{z}{z_0}\right) dz}{h - z_0} \tag{B-2}$$

The integral in the numerator of (B-2) can be approximated as follows, assuming that z_0/h is small:

$$\int \ln(cx)\, dx = x ln(cx) - x + c \tag{B-3}$$

$$\int_{z_0}^{h} \ln\left(\frac{z}{z_0}\right) dz = \left[z \ln\left(\frac{z}{z_0}\right) - z\right]_{z_0}^{h}$$

$$= \left(h \ln\left(\frac{h}{h_0}\right) - h\right) - \left(z_0 \ln\frac{z_0}{z_0} - z_0\right)$$

$$= \left(h \ln\left(\frac{h}{h_0}\right) - h\right) + z_0 \tag{B-4}$$

$$= h\left(\ln\left(\frac{h}{h_0}\right) - 1 + \frac{z_0}{h}\right)$$

$$= h\left(\ln\left(\frac{h}{z_0}\right) - 1\right)$$

* S. J. Smith, Unpublished. June 2018. Coastal and Hydraulics Laboratory, Engineer Research and Development Center.

Again, assuming that z_0 is small, the depth-averaged velocity is given as

$$\bar{u} = \frac{\frac{u_*}{\kappa}\int_{z_0}^{h}\ln\left(\frac{z}{z_0}\right)dz}{h-z_0} = \frac{u_* h\left(\ln\left(\frac{h}{z_0}\right)-1\right)}{\kappa(h-z_0)} = \frac{u_*\left(\ln\left(\frac{h}{z_0}\right)-1\right)}{\kappa} \tag{B-5}$$

To determine the value of z for which $u(z) = \bar{u}$:

$$u(z) = \bar{u}$$

$$\frac{u_*}{\kappa}\ln\left(\frac{z}{z_0}\right) = \frac{u_*\left(\ln\left(\frac{h}{z_0}\right)-1\right)}{\kappa}$$

$$\ln\left(\frac{z}{z_0}\right) = \ln\left(\frac{h}{z_0}\right) - 1$$

$$\ln\left(\frac{h}{z_0}\right) - \ln\left(\frac{z}{z_0}\right) = 1 \tag{B-6}$$

$$\ln\left(\frac{h\,z_0}{z\,z_0}\right) = \ln\left(\frac{h}{z}\right) = 1$$

$$\frac{h}{z} = e \Rightarrow \frac{z}{h} = \frac{1}{e} = 0.3679$$

or $z \approx {}^{h}/_{3}$

To compute bed stress, (B-1) is rearranged to yield

$$u_* = \frac{u(z)\kappa}{\ln\left(\frac{z}{z_0}\right)} \tag{B-7}$$

$$u_* = \frac{\bar{u}\,\kappa}{\ln\left(\frac{h}{ez_0}\right)}$$

or approximately

$$u_* \approx \frac{\bar{u}\,\kappa}{\ln\left(\frac{h}{3z_0}\right)} \tag{B-8}$$

Bed stress is given as

$$\tau_b = \rho u_*^2 \tag{B-9}$$

$$\tau_b = \rho\left(\frac{\bar{u}\,\kappa}{\ln\left(\frac{h}{ez_0}\right)}\right)^2 \tag{B-10}$$

$$\tau_b \approx \left(\frac{\bar{u}\,\kappa}{\ln\left(\frac{h}{3z_0}\right)}\right)^2 \tag{B-11}$$

Unit Conversion Factors

Multiply	By	To Obtain
bars	100	kilopascals
feet	0.3048	meters
inches	0.0254	meters
microns	1.0 E-06	meters
miles (US statute)	1,609.347	meters
ounces (mass)	0.02834952	kilograms
pounds (force) per square foot	47.88026	pascals
pounds (force) per square inch	6.894757	kilopascals
pounds (mass)	0.45359237	kilograms
pounds (mass) per cubic foot	16.01846	kilograms per cubic meter
pounds (mass) per cubic inch	2.757990 E+04	kilograms per cubic meter
pounds (mass) per square foot	4.882428	kilograms per square meter
pounds (mass) per square yard	0.542492	kilograms per square meter
square feet	0.09290304	square meters
square inches	6.4516 E-04	square meters
square miles	2.589998 E+06	square meters
square yards	0.8361274	square meters
yards	0.9144	meters

Acronyms and Abbreviations

AB	AquaBlok
CEC	cation exchange capacity
DOER	Dredging Operations and Environmental Research
ERDC	US Army Engineer Research and Development Center
EWN	Engineering with Nature
FGS	fine-grained sediment
SITE	Superfund Innovative Technology Evaluation
USACE	US Army Corps of Engineers
US EPA	US Environmental Protection Agency
WB	Willow Bend
XRA	X-Ray Attenuation

REPORT DOCUMENTATION PAGE

Form Approved
OMB No. 0704-0188

1. REPORT DATE	2. REPORT TYPE	3. DATES COVERED *(From - To)*
September 2020	Final Report	

4. TITLE AND SUBTITLE
Laboratory Evaluation of Aquablok™ Erosion Resistance: Implications for Geotechnical Applications

5a. CONTRACT NUMBER

5b. GRANT NUMBER

5c. PROGRAM ELEMENT NUMBER

6. AUTHOR(S)
Anthony M. Priestas, Charles F. McKenzie, John H. Hull, Reed Ellis, and Joseph Z. Gailani

5d. PROJECT NUMBER
485304

5e. TASK NUMBER

5f. WORK UNIT NUMBER

7. PERFORMING ORGANIZATION NAME(S) AND ADDRESS(ES)
Coastal and Hydraulics Laboratory
US Army Engineer Research and Development Center
3909 Halls Ferry Road
Vicksburg, MS 39180-6199

AquaBlok, Ltd.
175 Woodland Avenue
Swanton, OH 43558

8. PERFORMING ORGANIZATION REPORT NUMBER
ERDC/CHL SR-20-3

9. SPONSORING/MONITORING AGENCY NAME(S) AND ADDRESS(ES)
Dredging Operations and Environmental Research Program
Vicksburg, MS 39180

10. SPONSOR/MONITOR'S ACRONYM(S)
DOER

11. SPONSOR/MONITOR'S REPORT NUMBER(S)

12. DISTRIBUTION/AVAILABILITY STATEMENT
Approved for public release; distribution is unlimited.

13. SUPPLEMENTARY NOTES

14. ABSTRACT
AquaBlok™ (AB) is a commercial product traditionally used as an alternative material for contaminated sediment capping applications. Previous studies of AB capping performance have reported enhanced stabilization through increased erosion resistance. Subsequently, AB has been considered for use as an alternative levee repair material due to its cohesive properties. Through a series of laboratory experiments, this study investigated the erosion behavior of new AquaBlok formulations (10%, 20%, and 30% clay by weight) under increased shear stresses previously unachievable in the previous tests. The new AquaBlok formulations were tested in non-compacted and compacted states to simulate the physical properties in capping and levee repair applications.
In the non-compacted state, excess hydration of the clay matrix extended approximately 5 cm below the bed surface, which greatly reduced erosion resistance, and was independent of clay percentage. Below this horizon, critical shear stress increased, and erosion rates decreased, with clay percentage, respectively. However, this does not consider a continuous change in hydration state when exposed to free water. In the compacted state, erosion rates were greatly arrested, with measureable erosion only possible under the maximum applied shear stress (24 Pa). The results are discussed in the context of capping and levee applications.

15. SUBJECT TERMS
Earth dams—Erosion, Earth dams—Maintenance and repair, Levees—Erosion, Levees—Maintenance and repair, Materials—Erosion, Materials--Evaluation

16. SECURITY CLASSIFICATION OF:			17. LIMITATION OF ABSTRACT	18. NUMBER OF PAGES	19a. NAME OF RESPONSIBLE PERSON
a. REPORT	b. ABSTRACT	c. THIS PAGE			Anthony M. Priestas
Unclassified	Unclassified	Unclassified	SAR	65	19b. TELEPHONE NUMBER *(Include area code)* 601-634-2978